Universidade de Aveiro
Departamento de
Eletrónica, Telecomunicações e Informática

2014

Jorge Miguel Abrantes de Almeida Gomes

Amplificador de Potência em GaN para Comunicações via Satélite

(GaN Power Amplifier for Satellite Communications)

Universidade de Aveiro
2014
Departamento de
Eletrónica, Telecomunicações e Informática

Jorge Miguel Abrantes de Almeida Gomes

Amplificador de Potência em GaN para Comunicações via Satélite

(GaN Power Amplifier for Satellite Communications)

dissertação apresentada à Universidade de Aveiro para cumprimento dos requisitos necessários à obtenção do grau de Mestre em Engenharia Eletrónica e Telecomunicações, realizada sob a orientação científica do Professor Doutor Nuno Miguel Gonçalves Borges de Carvalho, Professor Catedrático do Departamento de Eletrónica, Telecomunicações e Informática da Universidade de Aveiro, e co-orientação do Doutor Pedro Miguel Duarte Cruz, investigador do Instituto de Telecomunicações de Aveiro

Dedico este trabalho aos meus pais, Maria e Fernando, pelo incansável apoio e carinho.

I dedicate this work to my parents, Maria and Fernando, for the constant support and care.

“A person who never made a mistake, never tried anything new.”
(Albert Einstein)

o júri/ the jury

presidente / president

Professor Doutor João Pedro Estima de Oliveira
Professor Associado da Universidade de Aveiro

vogais / examiners committee

Professor Doutor José Alberto Peixoto Machado da Silva
Professor Associado da Universidade do Porto

Professor Doutor Nuno Miguel Gonçalves Borges de Carvalho
Professor Catedrático da Universidade de Aveiro (Orientador)

Agradecimentos/ Acknowledgments

Em primeiro lugar quero prestar um enorme agradecimento a ambos os orientadores, ao Prof. Nuno Borges de Carvalho e ao Dr. Pedro Cruz, pelas ideias e pela ajuda prestada.

Em especial ao Dr. Pedro Cruz pela motivação e conselhos suplementares, por todas as críticas e opiniões que me apresentou ao longo do trabalho para que este chegasse a bom porto.

Ao Sr. Paulo Gonçalves pelo esforço adicional que este trabalho exigia e pelos conselhos na implementação prática.

Aos meus pais, Maria e Fernando, e à minha irmã, Ana Sofia, por me proporcionarem todas as condições necessárias ao longo destes anos e por ajudarem a construir o meu futuro com conselhos e ações. Sem eles nada disto se teria concretizado.

À minha namorada, Ana Rita, de uma forma muito especial pelo eterno carinho e pela inabalável confiança na minha pessoa.

Aos meus amigos, Frederico Malafaia, Bruno Silva e André Branquinho, e à equipa de futebol da sala de Sistemas Rádio do IT, pelos momentos de descontração ao longo deste trabalho.

A todos Muito Obrigado!

palavras-chave

Amplificadores de Potência para Rádio Frequência, Nitreto de Gálio, Comunicações via Satélite

resumo

As comunicações via satélite têm-se tornado uma alternativa válida às vias de comunicações convencionais, como a fibra e o cobre, em situações de catástrofe ou até como complemento para melhorar a qualidade de serviços disponibilizados à escala global. Recentemente, os engenheiros de rádio frequência têm trabalhado para encontrar uma solução definitiva e fiável para a substituição dos amplificadores a válvulas nos satélites de comunicações. Apesar destes amplificadores apresentarem uma performance de destaque, o seu tamanho, peso, consumo e custo são sérios problemas para as empresas especializadas na sua construção. Contudo, o panorama tende a mudar devido à exploração da tecnologia de Nitreto de Gálio em aplicações de alta potência, frequência e eficiência.

O objetivo desta trabalho passa pela implementação de dois amplificadores de potência em classe B, recorrendo a transístores de Nitreto de Gálio e usando diferentes linhas de transmissão planares, para a frequência de 5.8GHz que é frequentemente usada em transmissões *uplink* na banda C, ou mesmo nas recentes aplicações de transferência de energia sem fios.

Os melhores resultados foram obtidos pela implementação em linhas *microstrip*, atingindo os 34.1dBm de potência de saída, 62.35% de eficiência na saturação e um ganho máximo de 17dB.

keywords RF Power Amplifiers, Gallium Nitride, Satellite Communications

abstract

The satellite communications have become a valid alternative to conventional communications, through fiber or copper, in situations of catastrophe or even as complement to improve the quality of the services provided at a worldwide scale. Recently, radio frequency engineers have worked towards a reliable solution to replace the travelling wave tube amplifiers on board of the satellite communications. Despite the travelling wave tube amplifiers reveal a good performance, its weight, size and cost are a serious technical problem to the main satellite manufacturers. However, this scenario tends to change due to the exploitation of the Gallium Nitride technology in high power, efficiency and frequency applications.

The objective of this work involves an implementation of two power amplifiers in class B, resorting to a Gallium Nitride transistors and using different types of planar transmission lines, for a 5.8GHz frequency which is often used in uplink transmissions for C-band or even in recent applications of wireless power transmission.

The best results were obtained for the microstrip lines power amplifier, achieving 34.1dBm of output power, 62.35% of drain efficiency at saturation and a small-gain of 17dB.

Contents

List of Figures

List of Tables

Acronyms List

ACPR	Adjacent Channel Power Ratio
ADS	Advanced Design System
AlGaN	Aluminum Gallium Nitride
AlN	Aluminum Nitride
ARL	Army Research Labs
AT&T	American Telephone and Telegraphs
BIS	British Interplanetary Society
BER	Bit Error Rate
CAD	Computer Aided Design
CBPW	Conductor Backed Coplanar Waveguide
CPW	Coplanar Waveguides
CR	Cognitive Radio
CW	Continuous Wave
DBS	Direct Broadcasting Satellite
DSP	Digital Signal Processor
DUT	Device Under Test
ESA	European Space Agency
EVM	Error Vector Magnitude
FBH	Ferdinand-Braun-Institut für Höchstfrequenztechnik
FET	Field Effect Transistor
FM	Frequency Modulation
FPGA	Field Programmable Gate Array
GaAs	Gallium Arsenide
GaN	Gallium Nitride
GPS	Global Positioning System
HAC	Hughes Aircraft Company
HB	Harmonic Balance
HDTV	High Definition Television
IAF	Fraunhofer Institut für angewandte Festkörperphysik
IEMN	Institute d'Électronique de Microélectronique et de Nanotechnologie
IMD	Intermodulation Distortion
IMR	Intermodulation Distortion Ratio
InP	Indium Phosphide

IP3	Third Order Intersection Point
ITU	International Telecommunications Union
JAXA	Japan Aerospace eXploration Agency
LDMOS	Difused Metal Oxide Semiconductor
LNA	Low Noise Amplifier
LTE	Long Term Evolution
MMIC	Monolithic Microwave Integrated Circuit
MRI	Magnetic Resonance Image
NASA	National Aeronautics and Space Administration
OFDM	Orthogonal Frequency Division Multiplexing
PA	Power Amplifier
PAE	Power Added Efficiency
PAPR	Peak to Average Power Ratio
PSK	Phase-Shift Keying
QoS	Quality of Service
QAM	Quadrature Amplitude Modulation
RAF	Royal Air Force
RF	Radio-Frequency
SAR	Synthetic Aperture Radar
SDR	Software Defined Radio
SiC	Silicon Carbide
SMD	Surface Mounted Device
SSPA	Solid State Power Amplifier
SSPS	Space Solar Power System
TEM	Transverse Electromagnetic
TWTA	Travelling Wave Tube Amplifier
USA	United States of America
WPT	Wireless Power Transmission
VoD	Video on Demand
VoIP	Voice over Internet Protocol
VSA	Vector Spectrum Analyzer
VSG	Vector Signal Generator

1. Introduction

1.1. Historical Review of Satellite Communications

Everything began in 1945, when a Royal Air Force (RAF) electronics officer and member of the British Interplanetary Society (BIS), Arthur C. Clarke, published an article in the British magazine Wireless World describing how could be placed on a geostationary orbit an artificial satellite that would forward the radio signals to different places on Earth, establishing communication between them, even if they were not in line of sight. The concept introduced by Arthur C. Clarke went further beyond, and so he suggested the launch of three satellites to geostationary orbits located above the heavily populated areas of United States of America (USA), providing direct broadcast television [1]. Strong political and economic factors were the major impediments to the development of such visionary idea. Although Arthur C. Clarke have repeated its formulation in 1951/1952 in The Exploration of Space, no one was interested about its exploitation.

John R. Pierce (figure 1), from America Telephone and Telegraph's (AT&T's), published in 1955 an article entitled Orbital Radio Relays, where he presented a well elaborated study about the utility of satellite communications and highlighting Clark's concept (space mirrors or space relays). Comparing, posteriorly, the capacities of the satellite communications systems and the transatlantic telephonic cable (TAT-1) that had been installed in the previous year, he predicted that the satellite communications could lead towards a billion dollar business. Later on, John R. Pierce and Harold A. Rosen (figure 2) from Hughes Aircraft Company (HAC) would be considered, by Arthur C. Clarke, the true pioneers of the satellite communications [2].

Figure 1 - John R. Pierce (from [3])

Figure 2 - Harold A. Rosen (from [4])

One decade later (1957), the dream of Arthur C. Clarke was materialized when the former Soviet Union launched the first artificial satellite called Sputnik I (figure 3). Its mission was simple and consisted in transmitting a beep with frequency between 20MHz and 40MHz to be synchronized by the radio ham operators [5]. After 22 days in orbit, its battery ran out and when it was reentering in Earth atmosphere, the Sputnik burned.

This step taken by former Soviet Union woke up the American superiority complex and Sputnik I became a serious case of study. The AT&T's and the HAC in collaboration with National Aeronautics and Space Administration (NASA) had a very important role in several projects focused on the development of the first American satellites, such as TELSTAR (figure 4) which was responsible for the first live television images between USA and France, and SYNCOM which transmitted the Summer Olympic Games from Japan to USA in 1964 [2].

Figure 3 - Sputnik I (from [6])

Figure 4 - TELSTAR (from [7])

1.2. Today's Satellite Communications

Many years passed since the first transmissions and nowadays satellite communications have gained a prominent position in localization, navigation, telecommunications, radar and weather systems. Many companies were founded all around the world, such as Eutelsat and Inmarsat in Europe, Telesat and EchoStar in America, with the original aim of exploiting this rentable business.

In the last few years, the satellite communications have become a support to the conventional cable (copper and fiber) and wireless systems. Even in the broad era of the wideband optical fiber and internet, there is a need to solve engineering problems related with the communication access from and to remote spots across large continents and oceans [8]. Using the conventional technologies mentioned before, the cost of copper or fiber would be prohibitive and the poor performance of the entire system would be unacceptable.

The benefits of satellite communications have steadily expanded its usage in the telecommunications area. For instance, a small group or satellite constellations can cover a much vaster area than terrestrial networks because they always need specialized infrastructures that can be outdated or insufficient. Even more, a satellite network can provide constant and uniform quality of service (QoS) regardless the type of network topology, geography of terrains and level of congestion and latency inside the network. In contrast, the performance of terrestrial networks are heavily affected by the variation of these parameters. In addition, the satellite connections are extremely scalable and thus, the satellite network can be easily reduced or expanded, answering quickly to new requirements.

1.3. Applications of Satellite Communications

The growth of the demand for services with better quality and robustness, for high density population areas, led to the increasing usage of satellite communications. Consequently, it has been verified that satellites actually carry all kind of data around the world, particularly the recent commercial contents such as High Definition Television (HDTV), digital radio, internet trunking and other broadband mobile services [9]. Satellites are also on the frontiers of such advanced applications as telemedicine, distance learning, Voice over Internet Protocol (VoIP) and Video on Demand (VoD). In addition to that, in military applications [10], a typical usage of such satellites is the restoration of communication capability in case of disasters: In case of a major disaster as the Katrina Hurricane (USA, 2005), the earthquake and tsunami in Chile (2010) and in Japan (Fukushima, 2011), all communication means were severely damaged over a long period of time. But, even smaller disasters as Klaus (France, 2009) have a serious impact on telecommunications. This includes classical voice over fixed and mobile networks but also all classical internet access methods except satellite. A constellation of small satellites on low altitude orbits can be used to restore the communication capability very quickly and enable rescue operations in good conditions for a short-term. The design of such a constellation has been proposed in [11], leading to a small constellation that could be launched within a day period.

Although these innovative steps taken by satellite communications in recent years, the experienced everyday breakthroughs are not made to replace the conventional networks. The aim is combining the two worlds and provide more and better services in a worldwide scale.

The satellite communications have an exclusive portion of spectrum located fundamentally between 1GHz and 40GHz which is subdivided in small frequency bands that are named differently (see Table I).

Table I - Satellite Communications spectrum bands (modified from [12, 13])

Band	Frequency(GHz)	Main applications
S	1-2	Global Positioning System (GPS) carriers, satellite radio, satellite mobile phones
L	2-4	Weather radar, surface ship radar, some communication satellites
C	4-8	Full-time television satellite networks, raw satellites feed
X	8-12	Military, civil and government applications, weather monitoring, air traffic control, maritime traffic control, vehicle speed detection
Ku	12-18	Satellite communications
Ka	26-40	High resolution, close range targeting radars on military aircraft

1.4. RF Payload Limitations

The lower frequency bands are becoming increasingly congested, so in the last couple of years other solutions have been exploited to occupy the upper frequency bands (for example Ka Band). The upper frequency bands are very attractive because the main objective is relieve the congestion of services accumulated in lower bands and at the same time allocate the modern applications that require larger bandwidths [14].

Ka band is the last frequency band which received a huge amount of money for research, because it is necessary to develop a supported technology that is capable to operate at very high frequencies and provide good performance characteristics as power and efficiency in radio frequency (RF) circuits with reduced dimension. New antenna approaches combined with the proper power amplifiers (PAs), can offer the real drive necessary to fulfill the requirements in Ka band. For instance, active multifeed and multibeam antennas can generate the overall output power by active beamforming. On the other hand, the breakthroughs sensed in software defined radio (SDR) and cognitive radio (CR) promise more efficient and flexible approaches to truly generalized radios front-ends that are able to use whichever communications waveforms [9]. Thus, the research is also centered in the digital processor, the heart of this reconfigurable payload, because it manages the connectivity by configuring the analog front-ends and treats the data by adjusting the frequency operation of the channels. This element allows potentially maximize the payload bandwidth and the power utilization over satellite lifetime. However, the performance of the reconfigurable payloads strictly depends on the performance of the higher power section. So, as the PA is the most important part in the payload architecture, because it

determines the overall efficiency and the amount of power to satisfy the link margin at the RF front-end, the development sensed in PAs technologies are emphasized in the next paragraphs.

In the space domain, the Travelling Wave Tube Amplifiers (TWTAs) (figure 5) and Klystron Amplifiers continue to cover the majority of the amplifying stage onboard of satellites [15]. Until the 70's, all satellites and earth stations dedicated to satellite communications included, in its system architecture, a PA belonging to this category due mainly to its capability to handle with high power levels combining also high linearity and efficiency required to establish communication links from and to Earth using multicarrier signals [15]. In other words, the TWTAs are components that allow to achieve the claimed performance for this type of communication links, but due to its constant working, they need a high supply voltage (in the order of several thousands of volts) that diminishes their reliability. Furthermore, every solutions based on these technologies are expensive, heavy and big aspects which are not appreciated by the satellite industry.

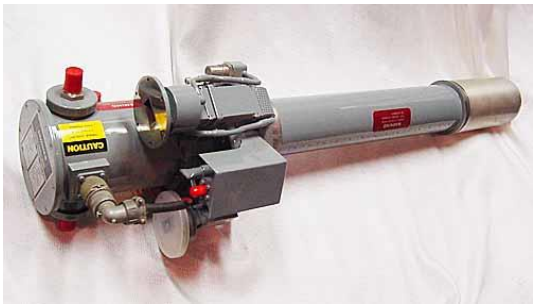

Figure 5 - TWTA (from [16])

So, in the last 30 years, RF engineers have been working on optimization of satellite communications infrastructures and there have been many attempts to replace gradually the TWTAs by Solid State Power Amplifiers (SSPAs) produced mainly within the Gallium Arsenide (GaAs) technology. However, as GaAs technology is limited in terms of power density and the capability to provide high power levels, TWTAs are still used in high power and high frequency applications [16].

Recently, a new solid state technology started to change this figure. This technology is called Gallium Nitride (GaN) and it is becoming a major solution when high power is the goal, at least for terrestrial applications. GaN technology presents several advantages [17]:

- high power density;
- increased efficiency over frequency;
- ability to maintain high performance over wide bandwidths;
- immunity against radiation;
- excellent thermal dissipation;

- high voltage operation;

GaN technologies appear to be a key element for the future of space industry. For instance, due to the high power density of GaN devices, it can be achieved a given power target with much less combining of power amplifiers. Thus, the satellite communication systems will have advantages of compact size, low mass and low cost, suitable for low-cost small satellites where the physical size, mass, power consumption and cost pose serious restrictions. In the example shown in the figure 6, it would be necessary to combine four 6.5W Ku-band GaAs PAs to achieve the same 20W power target that a single GaN PA can achieve. Consequently, the reduced combining leads to lower system losses as well.

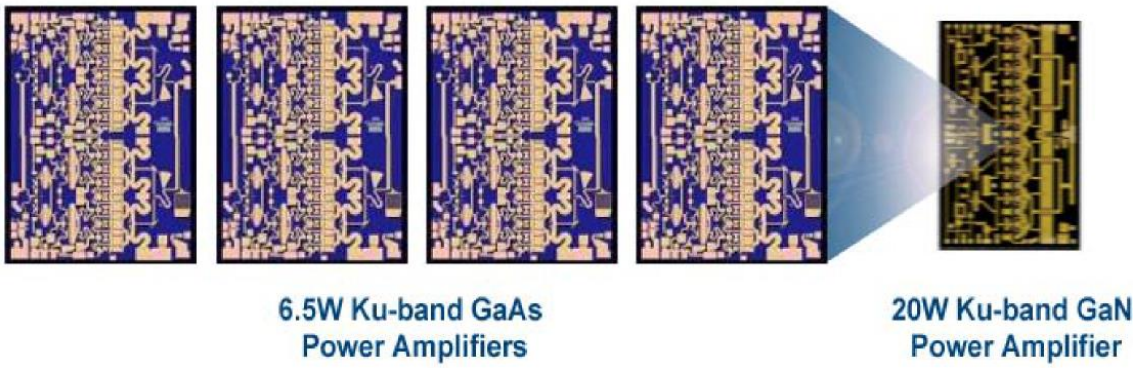

Figure 6 - Comparison of size for identical PAs based on GaAs and GaN (from [18])

This progress will be a significant step beyond the state of the art, and will open the door for GaN-based SSPAs into various space applications such as satellite communications, direct broadcasting satellites (DBS) and synthetic aperture radars (SAR).

1.5. State of the Art

As mentioned before, the TWTAs are still widely used in satellite communications at high frequencies, because they can provide a high power, linear and efficient output [19]. The TWTAs specifications can be summarized as kilowatts of output power for S, L, C and X-band applications and hundreds of watts for Ku and Ka band, 750W and 500W respectively [20,21]. The overall efficiency is typically 50% [22] and their weight varies according to the type of application, but it is normally comprised between 20 and 60 kg. Besides the TWTA weight, its power consumption, around a few kilowatts [20-22], is another serious drawback to be considered.

The SSPAs based on GaAs technology, used mostly until C-band frequencies, exhibit similar performances to TWTAs [23], but only reach unit of watt to higher frequencies [24].

However, the satellite communications have experienced a significant development, especially in the last decade with a recorded average growth of 10.7% per year [25]. Large sums of money have been injected by the telecommunications and space industries in 2012 (figure 7) exceeding largely one hundred billions of dollars. All this investment has been channeled to research in wide band-gap semiconductors which are the main part for high power applications.

Figure 7 - Relative market sizes of the telecommunications, space and satellite industries (from [25])

There are several leading candidates to revolutionize the SSPAs, especially the field effect transistors (FETs) based on Aluminium Gallium Nitride (AlGaN)/GaN technologies [26] that offer a few features appreciated in satellite communications or in other high power applications. Table II shows a comparison between the GaN technology and others that are in a mature position, such as GaAs and Indium Phosphide (InP).

Table II - Comparison between material parameters for GaAs, InP and GaN (from [27])

Characteristic	GaAs	InP	GaN
Band-gap energy (eV)	1.43	1.34	3.40
Saturation velocity (m/s)	10^5	0.9×10^5	2.7×10^5
Critical breakdown field (MV/m)	40	50	330
Thermal conductivity (W/mK)	50	69	170
Cut-off frequency (GHz)	400	365	275

As highlighted in table II, GaN has higher critical breakdown field that allows operations under high supply voltages, being able to provide high power levels. The high saturation drift velocity, compared to GaAs and InP materials, minimizes the internal delays experienced by the devices which is fundamental to high frequency operation. The better thermal conductivity implies more power handling capability, reduced cooling requirements and a long lifetime. However, GaN has a lower cut-off frequency in face to other technologies, but its power density is higher which corroborates again its better performance when included in high power applications.

Initially, the technologies based on AlGaN/GaN were very promising, but an utopic reality, because its manufacturing process was frequently associated to expensive substrates as sapphire, and so this technology was relegated to be applied in other kind of applications as the military field (high security communications systems, electronic warfare, radar, etc) [28]. However, the bulky investment sensed leads to the technology maturity and allows the production of lower cost but equally high performance substrates as Silicon Carbide (SiC) or Aluminium Nitride (AlN), taking the GaN technology to a new level, being assumed as the main candidate for the next generation of high power applications.

The GaN importance to the future of space applications has been recognized and so several European projects have been initialized as the "GaN Reliability Enhancement and Technology Transfer Initiative" (GREAT) from European Space Agency (ESA) and "AlGaN and InAlN based microwave components" (AL-IN-WON) [29]. The main objective of these projects is to accomplish intensive tests to GaN technology in order to attempt the production of elements capable of exploiting properly all the potential of the higher frequency bands.

Although, GaN technologies at Ka band are still at an early stage of development in Europe, USA and Japan have recently made lots of progress on this, including the development of a corresponding monolithic microwave integrated circuit (MMIC) technologies.

In Europe some work at Ka band and higher frequencies has been successfully achieved by Institute d'Électronique (IEMN) in Lille and Fraunhofer Institut (IAF) in Freiburg. At Ferdinand-Braun-Institut (FBH), a robust X-band MMIC process is available which currently acts as the baseline process for the on-going Ka band MMIC developments on frame of the GaNSAT project.

The American company TriQuint and the Japanese company Toshiba are playing a key role in commercializing GaN Ka band MMICs. Additionally, at the Army Research Laboratory (ARL) in the USA, a Ka Band GaN process has been developed recently. This work performed at various research institutions demonstrates that the rush to solid state power Ka band devices has already started worldwide. For instance, during the last two years, Toshiba published a few papers on GaN Ka band [30, 31] showing some technological details of these devices. Peak output power levels of 15 W were shown and at a power level of 9 W, a power added efficiency (PAE) of 13% was obtained. These devices have been the building blocks for Toshiba's Ka band MMICs for satellite communications applications which were announced in [32].

Similarly, TriQuint presented a paper on 4.5-6 W single-ended and 8-9 W balanced power PA MMICs [33], and benchmarked these results. A PAE of 25% was achieved in Ka band. Finally, ARL are also very active in Ka band MMIC development. In [34, 35] they showed two stage MMICs with an output power level of 5 W and a PAE of 23%. As these works were focused mostly on circuit design, modelling and linearity issues, only a few technology details were presented.

Even in lower frequency bands the research did not stop and there have been some attempts to reach higher power and efficiency levels in order to replace definitely the TWTAs onboard of satellites. Fujitsu showed in [36] two PAs based on GaN, using a three stages technique for impedance transformation. One for C-Band where could be extracted 343W of output power with 53% of PAE and another one for X-band that could reach 101W of output power with 53% of PAE. Mitsubishi presented a paper in [37] which described a PA based on GaN for Ku-band. Using advanced techniques of harmonic control to high efficiency, the PA reached an output power of 60W and a PAE of 45%.

At higher frequencies such as Ku and Ka bands, the output power and efficiency from individual GaN devices are rather low. However, it is possible to have a SSPA based on GaN that will provide high power at high frequency bands. This will be achieved by exploiting the recent development in spatial power combining technologies, in which it is expected that a power output of several hundreds of watts at high frequency bands will be achievable.

Spatial power combining techniques have been of interest for many years, as they provide the means to combine the power from an increasing number of millimeter-wave sources using free space or air as power combining medium within a guided wave structure, avoiding losses in transmission line distribution and combining networks [38]. For a small number of power sources, the conventional structures for transmission and combining still present better efficiency. However, when the number of power sources increase substantially, the losses in feeding structures increase in a nonlinear relation and there is a certain number of power sources from which the losses are no longer acceptable (figure 8), influencing clearly the good performance of the system. For high frequencies, the cross-over point where the spatial combining becomes more efficient is still verified for a low number of power sources [38]. So, it is necessary to use a spatial combined structure that allows aggregating several power elements without losing efficiency.

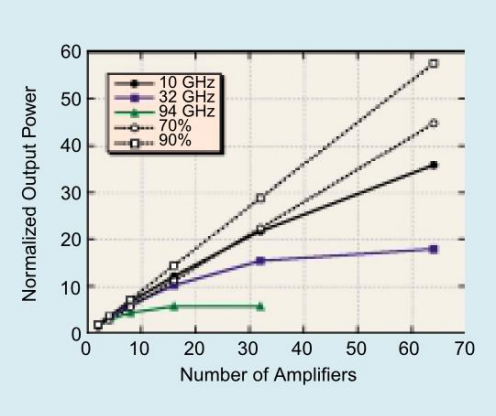

Figure 8 - Output power available from corporate and spatial power combining schemes versus the number of amplifier elements combined (from [38])

A significant progress has been presented in solid state space power combining in the last few years either in academic or in a corporate level. For instance, TriQuint bought recently the CAP Wireless and its ultimate technology, patented as Spatium. TriQuint has been in the frontline of the research performed in attempt to gather the state of the art of MMIC power devices and multiple element power combining techniques. Spatium technology uses finlines as power dividers/combiners of 8, 10, 16 or 32 PAs in order to produce high power and large bandwidth SSPAs. Some PAs using this technique are already in the market, standing out one for Ka-band that can deliver 150W of power, a PAE of 28% and a 3GHz of bandwidth and another one for Ku-band capable to deliver 250W of power, a PAE of 20% and 2.5GHz of bandwidth [39]. QuinStar Technology presented a paper in [40] which described a PA for W-Band combining 12 MMICs GaN amplifiers resorting to a radial-line combiner configuration. The 12-way combiner showed a efficiency of 87.5% and it was possible to design a PA able to provide 5W with a PAE close to 9% and a bandwidth of 5GHz. Researchers from Science University of Tokyo in partnership with some corporates as Panasonic Corporation and Japan Aerospace eXploration Agency (JAXA), developed a PA based on GaN for space communications for S-Band using circular waveguide combiners with an efficiency of 90%. Gathering all 8 MMICs, they obtained 1kW of delivered power and 50% of PAE for S-Band [41];

1.6. Objectives

This master thesis aims the understanding of the current state of satellite communications in nowadays telecommunications. Thus, it will be an introduction to this RF electronics field with a possible graduation in a future perspective.

In order to achieve this objective, the intention is getting familiar with transistors based on GaN technology, learning about the planar transmission lines commonly used in high frequency MMICs, the usual approaches for high efficient PAs and obtain some basic knowledge both in Computer Aided Design (CAD) tools for PA design and measuring instruments.

Due to technical limitations, it will not be produced a PA for the higher frequency bands in satellite communications as X-Band, Ku-Band or Ka-Band. Instead of that, they will be designed and produced two PAs for 5.8GHz frequency biased in class B with harmonic control, one using microstrip lines and other using coplanar waveguides (CPW).

The technical requirements defined to these PAs are the maximum PAE and power gain achievable and a minimum output power of 3W at 1 dB compression point.

The 5.8GHz frequency is exempt of license at the moment, so it can be used for relevant applications. One of them is related with satellite communications and corresponds to uplink transmissions for C-band. In fact, the broadcast community will join efforts with the satellite industry to safeguard C-band spectrum only for satellite services in front of International Communications Union (ITU) in World Radiocommunications Conference in 2015 [42].

Another application is intimately linked with Wireless Power Transmission (WPT). So, PAs operating at 5.8 GHz are a key issue for WPT applications such as space solar power systems (SSPSs) or the breakthrough concept of flying drones. SSPSs are considered one of the most promising renewable energy sources and estimations revealed an amount of power equivalent to a single nuclear power plant installed on Earth [43-46].

Daily, the potential of aerial drones is strongly highlighted and explored, but it is common sense the autonomy limitations of these devices. Using this frequency band, it can be developed and performed a system that allows to send energy into the free space to provide battery charging and data information during the flight.

1.7. Dissertation Organization

This master thesis is organized in several chapters chained in a logical manner to ease the access of all.

In the first chapter, it is presented the context and the motivation for this work. Furthermore, the structure of the thesis is also explained and the objectives are presented.

In the second chapter, there are some general notes about PAs. It will cover the usual figures of merit to evaluate the PA performance concerning on its linearity, gain, efficiency and stability. The classes of operation based on conduction angle are also described and there is a brief description about other approaches for highly efficient PAs.

In the third chapter are presented all the steps taken to design the two PAs and all the simulations done in Advanced Design System (ADS) in order to optimize and study the PAs performance.

In the fourth chapter, it is reported the details about the boards manufactured and, posteriorly, described all the measurements performed to both PAs. Then, some comparisons are made between the performance simulated and the results obtained.

Finally, the fifth chapter presents some conclusions and suggestions for future work.

During the elaboration of this dissertation, the author was congratulated with IEEE MTT-S Undergraduate Scholarship Spring 2014 (see Appendix A).

2. Power Amplifiers

The PA has an important role in micro and millimeter wave systems to several applications as the military (radar, improvised explosive device jamming), medical (magnetic resonance imaging (MRI), thermotherapy) and commercial (cellular base stations, personal mobile handsets, gateways, ground stations) [47].

On other hand, each application requires an exclusive set of requirements that makes the designed PA a unique part. For instance, the PAs used in satellite communications are strongly focused to reach certain efficiency levels, but the PAs suggested to MRI are more interested in large linearity and less efficiency [47].

Thus, the type of application where the PA will be integrated imposes different requirements of linearity, efficiency or power gain which are inevitably associated to the distinct classes of operation described in RF literature. On the other hand, the stability is another important concept that cannot be forgotten in order to avoid a useless system.

2.1. PA Figures of Merit

2.1.1. Linearity

Opposed to what is taught in the most part of engineering undergraduate courses, mainly in control and systems area, the nonlinear systems are the basic rule in engineering systems in contrast to the linear systems. The PA design also obeys to this principle and they are considered the part of the system that introduces more nonlinearities in communication systems [48].

The nonlinearities produced can be explained having in mind the basic principle for PA working based on energy conservation represented in figure 9. Thus,

$$P_{DC} + P_{in} = P_{diss} + P_{out} \tag{2.1}$$

where P_{DC} is the available power on supply source, P_{in} is the available power on the signal source, P_{diss} is the dissipated power by PA and P_{out} is the delivered power on the load. Defining the power gain as

$$G = \frac{P_{out}}{P_{in}} \tag{2.2}$$

But G can also be defined by,

$$G = 1 + \frac{\left(P_{DC} - P_{diss}\right)}{P_{in}} \tag{2.3}$$

Which it is deduced from equation (2.1).

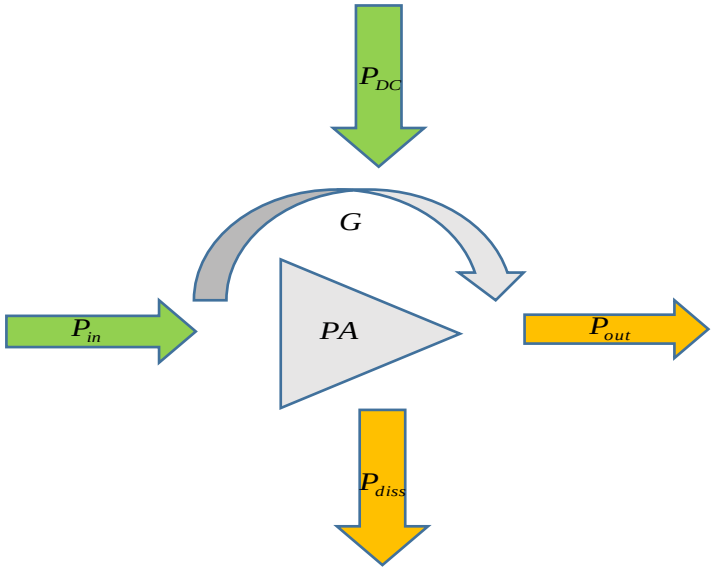

Figure 9 - PA power balance

Being a device whose main objective is to guarantee the increase of the input power level, the PA would be linear if for any input signal, the power gain verified in its output remained constant. However, this condition would just occur if the available DC power on supply source was inexhaustible and there were no dissipated power. Thus, increasing the input signal, the PA cannot provide output power correspondently to the linear power gain. This latter is going to decrease after a certain input signal level.

A. 1dB Compression Point

This is one figure of merit used to evaluate the PA linearity. It allows to find out how far the PA is quasi linear and from which point the PA is highly nonlinear. At low power levels, the output power level is increased by the small signal gain of the PA. This produces a quasi linear output versus input with ideal slope=1. At higher power levels, the PA begins to generate some power for nonlinearities and to compress the output signal. The result is gain reduction, commonly referred as gain compression. In conclusion, the 1dB compression point corresponds to the point where the small signal gain of the PA is 1dB below the small signal gain in case of

being always linear, regardless of the input level (figure 10). This figure of merit also represents and characterizes the AM-AM response of PA.

In other applications such as radar and WPT, 3dB and 5dB compression points are often used to characterize the PAs employed.

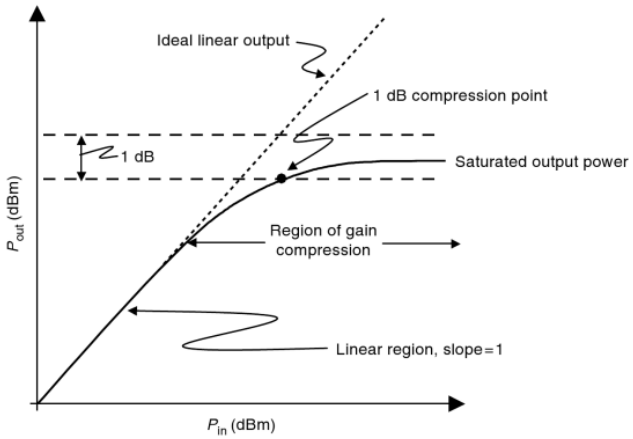

Figure 10 - Output power versus input power at the fundamental frequency for a nonlinear PA (from [49])

B. Intermodulation Distortion Ratio

When a RF signal is constituted by several well defined spectral frequencies, the PA will generate in its output new spectral components due to the intermodulation distortion products. The intermodulation components are the result of the sum and difference between all the harmonics that are part of the input signal. So, the intermodulation products features from PA are a very important aspect in real communication systems because they produce undesired components either inside the transmitted signal channel or in adjacent frequency channels where there are other independent RF signals that must not be disturbed. In order to understand this concept, if a two-tone signal is applied at PA input,

$$x(t) = A_1 \cos(\omega_1 t) + A_2 \cos(\omega_2 t) \tag{2.4}$$

The distortion components generated from this excitation are described in table III.

Table III - Intermodulation distortion products until the third order from a two-tone excitation

Mixing Product Order	Frequency
1^{st}	ω_1, ω_2
2^{nd}	$\omega_1 + \omega_2, \omega_2 - \omega_1$
3^{rd}	$2\omega_2 - \omega_1, 2\omega_1 - \omega_2, 2\omega_2 + \omega_1, 2\omega_1 + \omega_2$

In respect to intermodulation distortion (IMD) products, the odd order products require special attention (figure 11). They always settle down very close to the fundamental components of the transmitted signal and, particularly, the third order components are the ones which provoke the highest distortion in original signal (figure 12). One metric used to assess the distortion caused by the third order products is the intermodulation distortion ratio (IMR) which is defined by the ratio between the power of the fundamental signal and the worst IMD component which are frequently the third order products:

$$IMR = \frac{P_{fund}}{P_{3rd}} = \frac{P(\omega_1)}{P(2\omega_1 - \omega_2)} = \frac{P(\omega_2)}{P(2\omega_2 - \omega_1)} \tag{2.5}$$

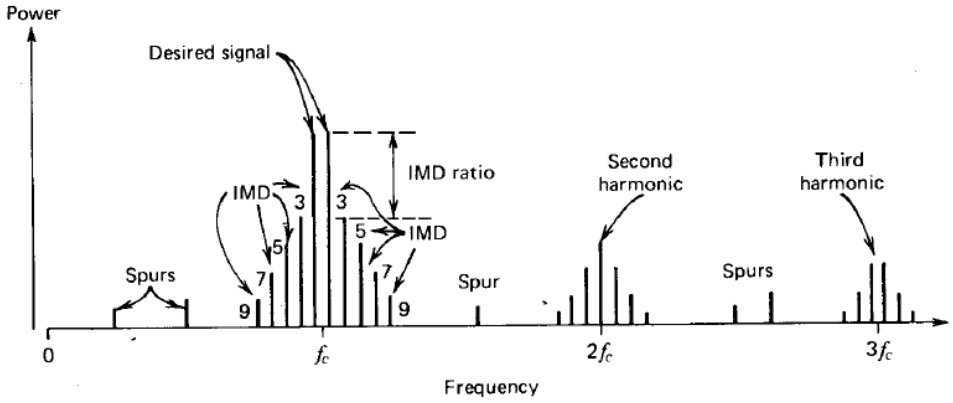

Figure 11 - Distortion products in a RF PA with two-tone excitation (from [50])

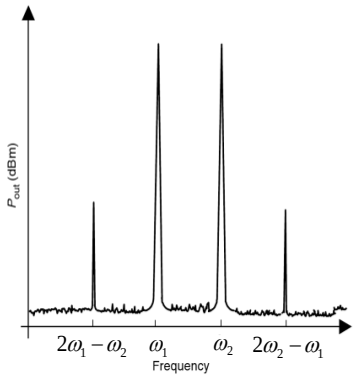

Figure 12 - An illustration of signal spectrum due to intermodulation distortion from two signals at frequencies ω_1 e ω_2 (from [49])

C. AM-PM

The AM-PM consists in the characterization of the phase variation in output signal according to changes of the input signal amplitude for a constant frequency, i.e., the amount of

the undesired phase deviation that is caused by amplitude deviations of the system. AM-PM conversion is usually defined as the change in output phase for a 1dB increment in the power sweep applied to the amplifier input.

AM-PM conversion is a critical parameter in systems where phase modulation is used, such as Phase-Shift Keying (PSK) or Quadrature Amplitude Modulation (QAM), because it provokes analog signal degradation. Consequently, the measured bit-error rate (BER) in the digital communication system increases.

The error vector magnitude (EVM) quantifies the performance of a radio transmitter against an ideal reference (figure 13). A signal sent by an ideal transmitter would have all the points in the I-Q constellation precisely placed at the ideal locations (the magnitude and the phase would be exact). In contrast, the nonlinear behavior of the transmitter, causes the constellations points fall in other locations distant from the ideal one.

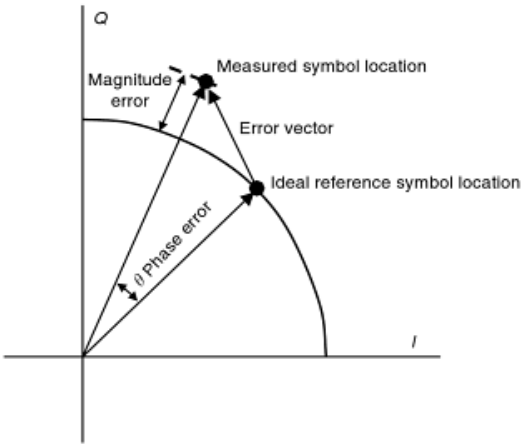

Figure 13 - I-Q diagram indicating the EVM measurement (from [49])

D. Third Order Intersection Point

When the input power increases, the harmonics power rise at a higher rate than the fundamental component power does. Normally, the power of the n^{th} harmonic increases n times faster than the fundamental component power. As the third order products are often characterized, there is one special point called third order intersection point (IP3) wherein the fundamental power curve intersects the third order component power curve, allowing the evaluation of the PA linearity. This is an imaginary point that results from the extension of both curves (figure 14), since these curves are going to compress after a certain input power level. The IP3 is related with the IMR through the expression 2.6.

$$IP_{3_{dB}} = \frac{1}{2} IMR_{dBc} + P_{out_{dB}} \tag{2.6}$$

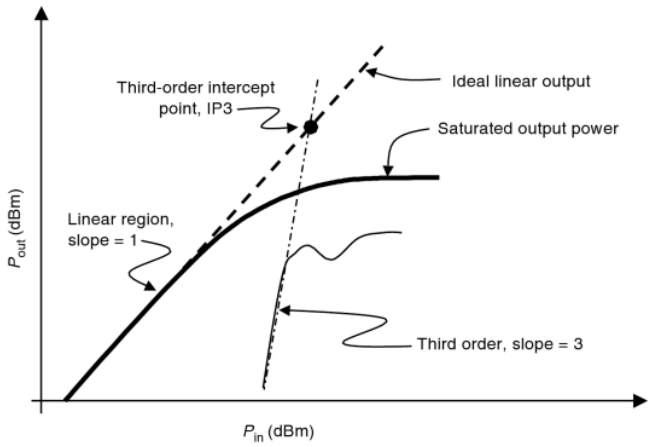

Figure 14 - Relationship between signal output power and intermodulation distortion product levels (from [49])

E. Adjacent Channel Power Ratio

Other figure of merit very common to assess PA linearity is the adjacent channel power ratio (ACPR), which is the amount of power that leaks into adjacent channels due to the nonlinearities created by PA when a modulated signal is transmitted. The interference level induced in adjacent channels grows as the input power level rises. This phenomenon is named by spectral regrowth (figure 15). Thus, the ACPR is usually defined as the ratio of the average power in the transmitted frequency channel to the average power in the adjacent frequency channel (upper or lower):

$$ACPR_{UA} = \frac{P_o}{P_{UA}} = \frac{\int_{\omega_{L2}}^{\omega_{U1}} S_o(\omega)\partial\omega}{\int_{\omega_{U1}}^{\omega_{U2}} S_o(\omega)\partial\omega} \tag{2.7}$$

$$ACPR_{LA} = \frac{P_o}{P_{LA}} = \frac{\int_{\omega_{L2}}^{\omega_{U1}} S_o(\omega)\partial\omega}{\int_{\omega_{L1}}^{\omega_{L2}} S_o(\omega)\partial\omega} \tag{2.8}$$

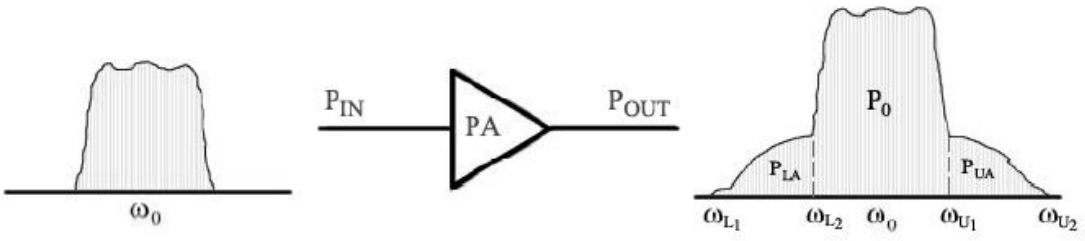

Figure 15 - Illustration of the spectral regrowth phenomenon (from [51])

Where ω_{U1} and ω_{L2} are the boundaries of the fundamental signal and, the $\omega_{U2}(\omega_{L2})$ and $\omega_{U1}(\omega_{L1})$ are the boundaries of the frequency spectrum of the upper adjacent channel (lower adjacent channel).

2.1.2. Efficiency and Power Added Efficiency

The PA performance rating is not only made by considering the amount of power delivered into the load by the PA. From the energetic point of view, the PA is a DC to RF converter and the existence of certain applications that are very inflexible in terms of energetic issues (for example, satellite communications mostly at the side of the satellite) is tightly compromised by the PA performance and, subsequently, the whole system. Thus, the comparison between several PAs also includes how much efficient they are when converting DC power to RF power. The PA efficiency is also denominated as drain efficiency in case of FETs and collector efficiency if a BJT is considered, and it is defined as follows:

$$\eta = \frac{P_{out}}{P_{DC}} \tag{2.9}$$

When the PA power gain is rather low, the contribution of P_{in} in P_{out}, cannot be neglected leading to wrong statements about PA efficiency. Thus, it arises another metric to describe the PA efficiency, named PAE and defined by:

$$PAE = \frac{P_{out} - P_{in}}{P_{DC}} \tag{2.10}$$

An important remark notices that for values of P_{out} much higher than P_{in} (power gain extremely high), the two expressions above end to the same results.

2.1.3. Power Gains

Several definitions for the PA power gain are presented in the literature. Considering a two port network (transistor) represented by its scattering matrix (S-parameters) and terminated by Z_S and Z_L in the appropriate ports (figure 16).

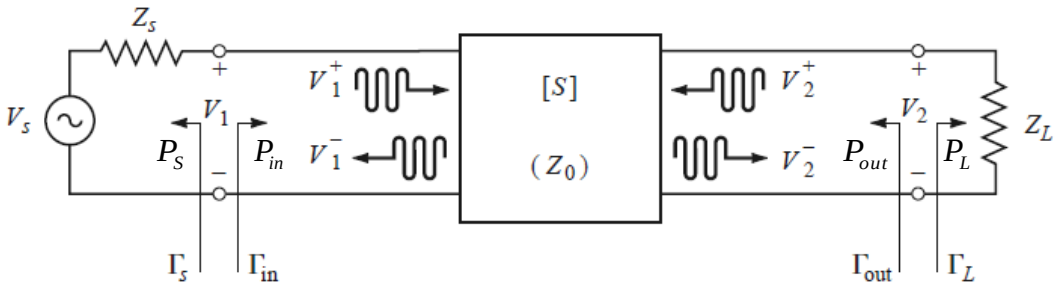

Figure 16 - A two port network with arbitrary source and load impedances (from [52])

- Operational Gain considers the ratio between the power delivered to the load (P_L) and the power available at the two-port network entrance (P_{in});

$$G_O = \frac{P_L}{P_{in}} \tag{2.11}$$

- Available Gain is the ratio between the power available at two-port network output (P_{out}) and the power available at the signal source (P_S);

$$G_A = \frac{P_{out}}{P_S} \tag{2.12}$$

- Transducer Gain is determined using the ratio between the power delivered to the load (P_L) and the power available at the signal source (P_S);

$$G_T = \frac{P_L}{P_S} \tag{2.13}$$

2.1.4. Stability Considerations

To aim a profitable PA design, it is necessary to guarantee the PA stability, namely how much the PA can resist to oscillation.

As the S-parameters are defined in terms of incident and reflected waves, the following equations can be written based on figure 16:

$$V_1^- = S_{11}V_1^+ + S_{12}V_2^+ \tag{2.14}$$

$$V_2^- = S_{21}V_1^+ + S_{22}V_2^+ \tag{2.15}$$

The oscillation is possible when the impedance seen into the input port or into the output port has a negative real part, which means $|\Gamma_{in}|>1 \text{or} |\Gamma_{out}|>1$. $|\Gamma_{in}|$ and $|\Gamma_{out}|$ are deeply related with the S-parameters of the two-port network and strongly conditioned by the chosen source and load impedances:

$$|\Gamma_{in}| = S_{11} + \frac{S_{21}S_{12}\Gamma_L}{1-S_{22}\Gamma_L} < 1 \tag{2.16}$$

$$|\Gamma_{out}| = S_{22} + \frac{S_{21}S_{12}\Gamma_S}{1-S_{11}\Gamma_S} < 1 \tag{2.17}$$

The PA is unconditionally stable for a certain frequency if for all passive impedances Z_S and Z_L chosen, the conditions above are fulfilled. In case of existence of any impedance that does not verify the same criteria, the PA is potentially unstable. These terms just guarantee the stability for one frequency (normally the nominal operation frequency), so there can be another frequency that drives the PA into oscillation mainly due to the designed matching networks. The named stability conditions, depict well defined regions in the Smith Chart, where the chosen Z_S and Z_L impedances lead to a stable PA. Thus, handling the inequalities above with the support of some mathematical operations, it is possible to deduce the center and the radius expressions to the stability circles for both input and output ports. So, this is a graphical method that allows to determine the frontier between the stable impedances and the potentially unstable impedances:

$$r_L = \left|\frac{S_{12}S_{21}}{|S_{22}|^2 - |\Delta|^2}\right| \quad C_L = \frac{\left(S_{22} - \Delta S_{11}^*\right)^*}{|S_{22}|^2 - |\Delta|^2} \tag{2.18}$$

$$r_S = \left|\frac{S_{12}S_{21}}{|S_{11}|^2 - |\Delta|^2}\right| \quad C_S = \frac{\left(S_{11} - \Delta S_{22}^*\right)^*}{|S_{11}|^2 - |\Delta|^2} \tag{2.19}$$

where $|\Delta| = |S_{11}S_{22} - S_{12}S_{21}|$. The stability circles center are marked with regard to the Smith Chart center. In case the stability circles do not include the Smith Chart center, the graphical method is interpreted, regarding to Γ_L plane, as follows:

- If $|S_{11}| < 1$ (figure 17 a)), the impedances outside the stability circles lead to a stable PA;
- If $|S_{11}| > 1$ (figure 17 b)), the impedances inside the stability circles lead to a stable PA;

Regarding to Γ_s plane, the procedure is similar but it is considered the $|S_{22}|$ instead of $|S_{11}|$.

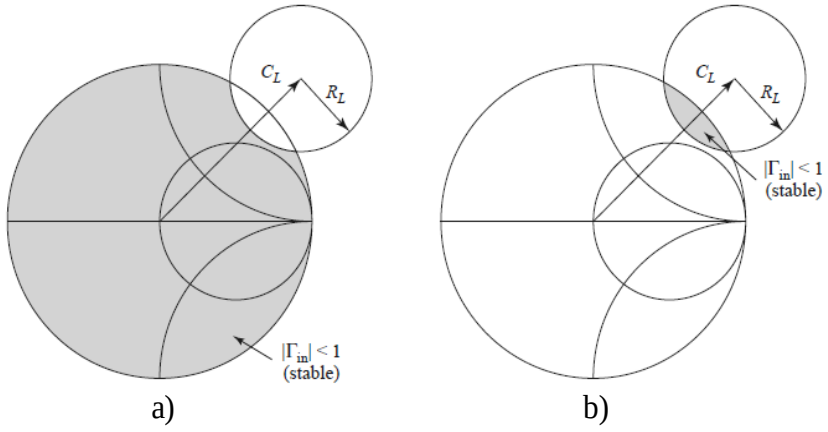

Figure 17 - Output stability circles for a conditionally stable device (from [52])

2.2. Classes of Operation

The operation classes, named by A, AB, B and C, are distinguished according to the different biasing point chosen for the active device. In these classes of operation, the active device assumes a current source role, controlled by a voltage in FETs or by a current in BJTs, driving signal for a confined range of input signal (figure 18).

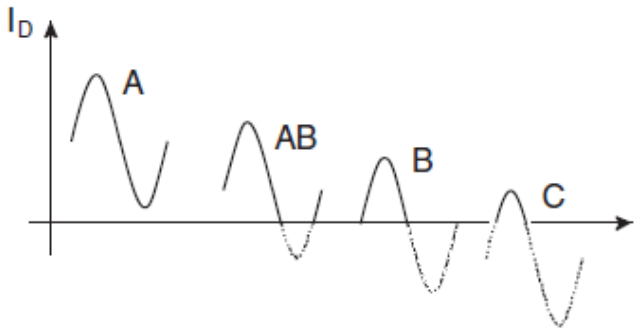

Figure 18 - Classes of operation defined as output current conduction angle (from [53])

In the specific case of class A, the active device drives signal for any value of the input signal, meaning that the output current waveform is a complete sinusoid (figure 18). Thereby, the class A has a conduction angle of 2π. The biasing point of class A is located in the linear region of the characteristic curve (figure 19) that results in the most linear operation class. However, as the active device is always driving signal, even in absence of input signal, the dissipated power is not null, so the efficiency is the lowest.

For the class B operation, the active device only drives signal for half range of the input signal. That results in a truncated output current waveform and a conduction angle of π. This behavior is due to the fact that the biasing point is near to the threshold point. Consequently, the class B linearity is lower than class A and the efficiency is higher because the active device does not dissipate power when there is no input signal.

All the biasing points located amid class A and class B lead toward to the class AB and a conduction angle between π and 2π. So, the efficiency level must increase, comparing to class A, and must be lower than in class B. Nevertheless, the class AB presents a better linearity than class B and a poor one relatively to class A.

Finally, the class C conducts for less than half cycle of the input signal due to the biasing point located below the threshold point. Thus, the class C is the most efficient operation class, but in contrast reveals the poorest linearity.

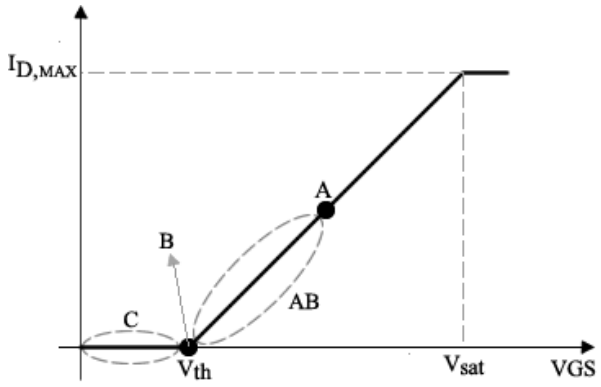

Figure 19 - Classes of operation located in I-V characteristic curve of a transistor (from [51])

Resorting to a few mathematical operations, it can be deduced, from the conduction angle definition [48], expressions to describe the output power (2.20), DC power consumed (2.21) and the efficiency (2.22) in terms of the conduction angle value, where V_1 and I_1 are the amplitudes of the fundamental components of the voltage and current respectively, and V_{DC} is the amplitude of the supply voltage:

$$P_{out} = \frac{1}{2} V_1 I_1 = \frac{1}{4\pi} V_{DC} I_{D_{MAX}} \frac{2\theta - \sin(2\theta)}{1 - \cos(\theta)} \tag{2.20}$$

$$P_{DC} = V_{DC} I_{DC} = V_{DC} \frac{I_{D_{MAX}}}{\pi} \frac{\sin(\theta) - \theta\cos(\theta)}{1 - \cos(\theta)} \tag{2.21}$$

$$\eta = \frac{P_{out}}{P_{DC}} = \frac{2\theta - \sin(2\theta)}{4(\sin(\theta) - \theta\cos(\theta))} \tag{2.22}$$

Clarifying the equation 2.22, the class A efficiency reaches a maximum of 50%. Decreasing the conduction angle, the efficiency rises, substantially, achieving 78.5% for class B and tending towards 100% for an active device strongly biased in class C, i.e., null conduction angle. Further on, it will be verified that the PA efficiency is not only pondered by the biasing point but also by the nature of signal that will be amplified. On the other hand, equation 2.20 reveals that when efficiency is increasing, the active device provides a lower output power, achieving a theoretical 0 Watts again for class C operation.

In order to applications that are looking for PAs with good linearity, as satellite communications, the operation class must be carefully chosen and must vary between class AB and class B. Although class C exhibits better efficiency, this operation class is not recommended due to the linearity problems that can constitute a serious drawback.

2.3. Classes for High Efficient PAs

In the previous section, the PA class is controlled by a change in the bias point (and thus varying the conduction angle). However, as it was seen, the efficiency values are not very attractive for systems with energetic constraints.

Other classes of PAs are considered to increase the PAE, employing the active device as a switch which means, when the transistor is ON, the voltage across is nearly zero and a high current is flowing through the device. When the transistor is OFF, the current is nearly zero and a high voltage is verified across the active device [53]. If the active device acts as an ideal switch (infinite resistance when ON and null resistance when OFF), there is no current and voltage simultaneously, and then the power dissipation is lower, maximizing the PAE. So, the classes presented next are named by switched classes.

- **Class D**

The class D PA was invented by P. J. Baxandall in 1959 [54]. The concept is shown in figure 20, where the active devices operate in phase opposition and during a half time period each one (50% of duty cycle). The series resonant circuit at the output is tuned for the fundamental frequency, filtering the harmonic components.

If the two active devices were ideal, a 100% efficiency was achieved. However, the practical class D implementations suffers from finite parasitic resistance, switching speed and drain capacitance [55]. Finite switching speeds takes the active device to active regions, conducting current. Even more, when each active device is turned on, the voltage across is not zero (the resistance is not null) and so, there are losses. In addition, the parasitic capacitance of each active device forces power dissipation during the transistor switching and this effect is more pronounced when the frequency increases.

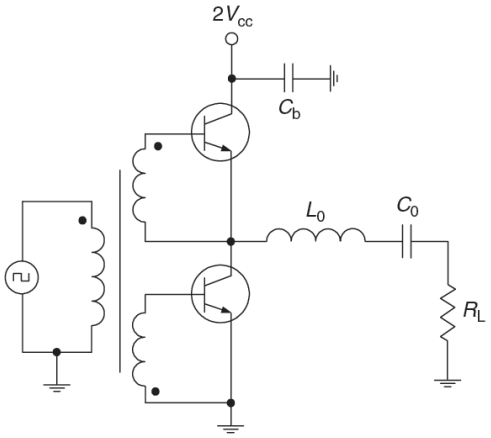

Figure 20 - Class-D in a complementary voltage-switching configuration (from [56])

- **Class E**

The class E PA was proposed by Nathan O. Sokal and Alan O. Sokal in 1975 [57]. This class solves the class D problem related to the power dissipation due to the parasitic capacitance and employs only one transistor acting as switch, connected to a series resonant filter at output (figure 21). In the ideal class E PA, the drain voltage drops to zero and maintains zero when transistor turns on, due to the coil L_1 that acts as a RF choke preventing the switching losses verified in class D. The result is a 100% efficiency.

However, the main problem of class E is related to the design of the output filter, which must fulfill a few important conditions: the first is the drain voltage that must be null when

transistors turns on, in order to avoid energy storage in the parasitic capacitance. The second is the first derivate of voltage must be also zero to prevent that efficiency drops [57].

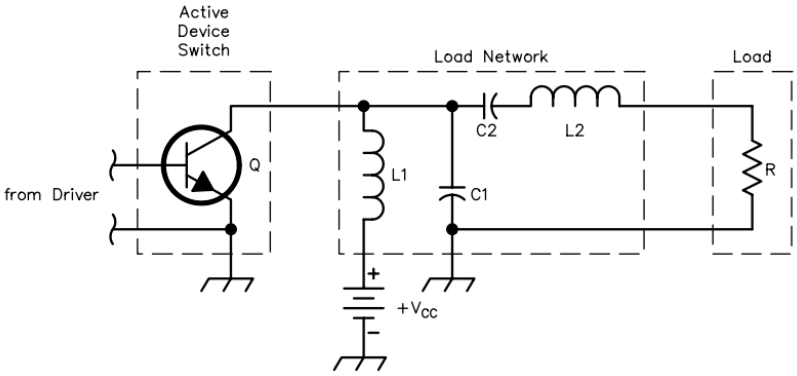

Figure 21 - Schematic of the Class-E PA (from [57])

- **Class F**

The class F characteristics make it a reliable solution when it is required to maximize the PAE. The class F is a well-known method for that purpose, presented in 1958 by V. Tyler. In fact, this class is not a true switching class, because the proper wave shaping for voltage and current is achieved by harmonic control, in contrast to class D and E referred previously, leading to an amplifier solution with a theoretical efficiency close to 100%.

The figure 22, shows a basic schematic of a PA operating in class F with the different harmonic terminations placed at the transistor drain. The output matching network in class F imposes that the odd harmonics are open-circuited and the even harmonics are short-circuited. This configuration produces results in a square voltage waveform (infinite sum of sinusoids) and a truncated current waveform. Consequently, the overlapping between these waves is reduced for the harmonics and, therefore, the dissipated power suffers a significant reduction and efficiency increases.

However, the class F reveals a problem related to the harmonic content. It is impossible to perform harmonic control for a high number of harmonics in practical implementations. So, the voltage waveform is no longer a perfect square wave, and then, dissipation is verified.

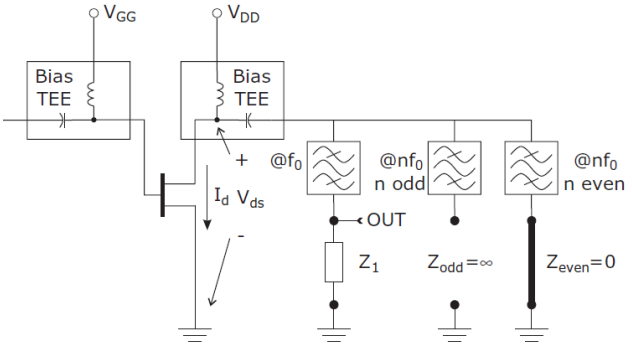

Figure 22 - Ideal schematic of a Class-F PA (from [53])

2.4. Other Strategies for PAs

With the evolution of telecommunications from 2G to 4G, new modulation schemes have been developed to attain fresh specifications related to transmission rates required by the modern applications. The new modulation schemes have a common characteristic: high peak to average power ratio (PAPR) precisely the type exhibited by WCDMA, CDMA2000, and systems employing Orthogonal Frequency Division Multiplexing (OFDM), such as WiMAX and Long-Term Evolution (LTE). That fact implies the PA will operate often near the signal average power (figure 23) and therefore its efficiency is considerable reduced [58]. Besides that, these recent modulations claim for linear amplification.

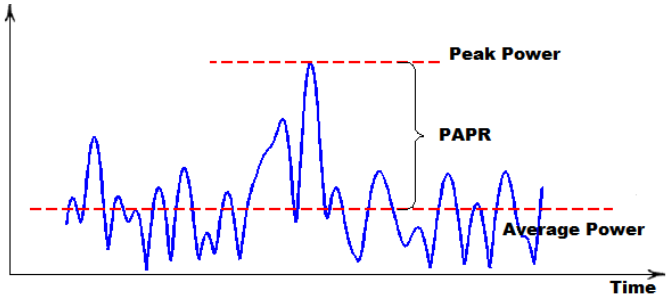

Figure 23 - Peak to Average Power Ratio of a random signal

Furthermore, the efficient conversion between DC power and RF power is always a key request especially in satellite communications where the DC power supply is limited and the power dissipation is considered a severe technical problem. The energetic issues constantly force a large economic investment in appropriated infrastructures and cooling systems plus the qualified labour, so it is absolutely necessary to take advantage of the maximum power available on system.

The PAs described in RF literature as highly efficient (class D, class E and class F) have seen their performance degraded by these high PAPR signals and by the distortion introduced as a consequence of their region of operation (mostly at saturation region), and they are replaced repeatedly by typical class AB or even class B to integrate communications systems mainly due to their high linearity. Nevertheless, the efficiency of class AB or class B is low and even lower for high PAPR signals. For instance, a typical class AB using Laterally Diffused Metal Oxide Semiconductor (LDMOS) transistors presents an efficiency between 8% and 15% when WCDMA waveforms are employed [59].

On the other hand, it was shown that higher PAPR signals bring benefits in WPT. Several works [60-62] have shown that the efficiency of the RF to DC conversion in the rectifier circuit placed in the receiver can be improved by selecting these type of signals for

excitation. Basically, as nonlinear RF to DC converters respond better to high amplitude signals, high PAPR signals (such as multisine signals) are able to excite them in a more efficient way, leading to higher DC output power levels. However, the WPT experiments have some problems concerning to energy transmission using these waveforms. WPT needs high gain and efficient PAs to take advantage of the peaks of these signals.

2.4.1. Efficiency

- ***Doherty Amplifier***

One alternative to achieve better efficiency in presence of signals with a high PAPR value is using an approach called Doherty PA. This configuration was firstly presented in 1936 by Doherty [63], as a means to counteract the poor average efficiency of class B PA. The main idea of this Doherty configuration appears when evaluating the operation of the class B designs when excited with signals with significant amplitude modulation. Class B PA are designed to achieve a maximum efficiency for a maximum input signal, and thus the load impedance is selected for that value, but when the signal is not maximum, then the PA reduces its efficiency, so the best approach was to consider a load that will follow the input signal excursion.

The main operation of a theoretical Doherty topology combines two PAs of equal capacity through quarter-wavelength lines or networks (figure 24). The carrier amplifier is normally set for a class B mode, while the peak amplifier is normally in a class C operation.

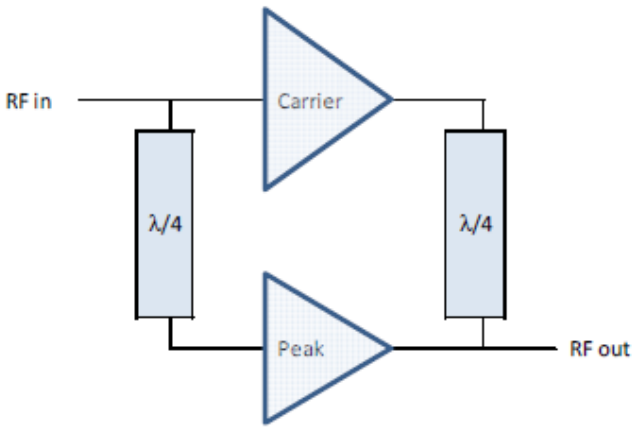

Figure 24 - Illustrative arrangement for a Doherty PA approach

When a high PAPR signal feeds the system, both amplifiers contribute to the output power in a non-symmetrical way: the carrier PA will amplify the signal when it has amplitudes close to the average power amplitude operating inside the linear region, while the peak PA

(normally cut-off to save energy) will be activated by the incoming peaks (carrier amplifier saturation limit), acting as a current source modulating the carrier amplifier load line.

The operation of the Doherty system can be understood by dividing it into low-power, medium-power (load modulation) and peak-power regions. So, in the low-power region, the instantaneous amplitude of the input signal is insufficient to overcome the class C bias, so the peaking PA remains cut-off and appears as an open-circuit. As the amplitude signal increases into the medium-power region, the carrier PA saturates and the peak PA becomes active. Thus, the increasing current injected by the peak amplifier into the common load to both amplifiers, causes the apparent load impedance at RF output terminal to increase. Transformation through the quarter-wavelength line results in a decrease in the load presented to the carrier PA. The carrier PA remains in saturation and acts a voltage source. The impedance reduction enables to reach more output power avoiding the clipping of the voltage waveform. As a result, a good efficiency is reachable for a wide range of input signal levels due to this dynamic load line according to the input signal envelope amplitude. At the peak-power region, both devices achieve their saturation and the efficiency curve tends to the class B efficiency (figure 25).

An other important aspect usually explored is the power division ratio at the RF input terminal. The use of other power division ratios allows the lower efficiency peak to be shifted leftwards, so the average efficiency is increased for signals with higher PAPR. However, when the lower efficiency peak is pushed to further power back-off levels, it becomes more pronounced when the peak amplifier starts to conduct.

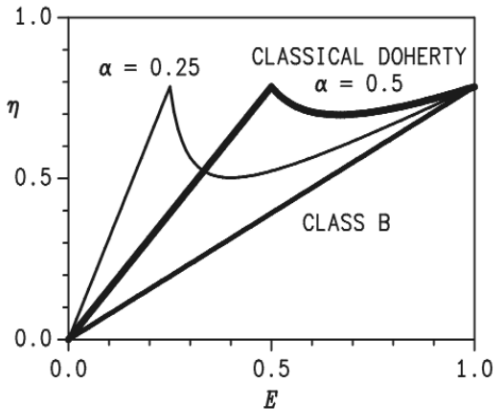

Figure 25 - Efficiency of the Doherty system compared with ideal Class-B PA (from [55])

- ***Envelope Tracking***

The first reference to this technique was made in 1929 when Loy Edgar Barton wrote an article explaining a way to reduce the excessive energy consumption of high power broadcast

transmitters. Meanwhile, this technique was forgotten due to the domain of frequency modulation (FM) transmitters.

With the existence of high PAPR signals, the DC power supply connected to the drain has a value greater than strictly necessary during most part of the operating time. Thus, the excessive amount of energy consumed is dissipated as heat by the PA (figure 26), taking the efficiency level to low values.

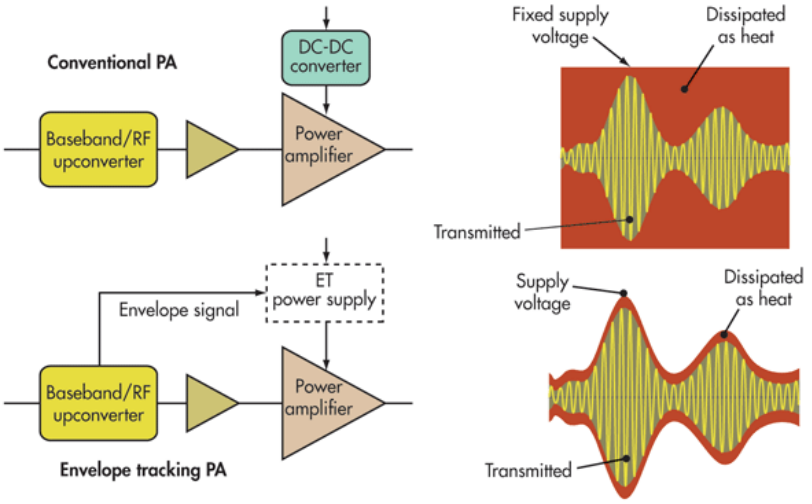

Figure 26 - Comparison between a conventional PA and an envelope tracking PA in terms of dissipated energy (from [64])

The solution proposed by envelope tracking technique is adjust the DC power according to the input envelope power, i.e., the supply voltage is dynamically varied in synchronism with the envelope RF signal to conserve power. Typically, the envelope signal is detected and used to control the power supply (DC-DC converter), and if the tracking of the envelope is perfect, the supply voltage preserves the peak efficiency of the RF PA. This technique benefits the PA efficiency, because it is going to operate close to saturation region as frequently as possible, and at the same time decreases the total energy wasted.

Figure 27 shows the drain efficiency trajectory as a function of the supply power voltage whose value is related with the signal amplitude. The output power of peak efficiency increases with the increase of the supply voltages, but has a constant high efficiency across a limited output power range to tolerate back-offs for high PAPR signals. In this manner, the PA is on the edge of the compression region more time. As illustrated, the effective drain efficiency is substantially higher than the actual drain efficiency of a PA with a fixed supply voltage (blue line).

2.4.2. Linearity

The PAs described before are used mainly to improve the average efficiency exhibited by PA. For power transfer applications, the nonlinearities, introduced by them, have no impact in the general purpose which is to transmit energy more efficiently as possible.

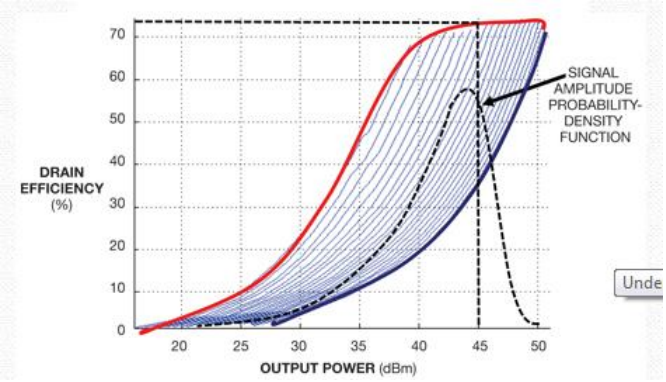

Figure 27 - Envelope Tracking efficiency concerning on the input signal envelope amplitude (from [65])

When systems are handling with information, the nonlinearities have collateral effects either in signal channel or in the adjacent transmitted frequency channels, which sometimes infringe the usage rules imposed. The linearity improvement costs efficiency, pushing the input power to back-off and the PA operates always in a linear region. In summary, efficiency and linearity are both mutually exclusive [66].

For instance, the Doherty configuration reveals some relevant problems concerning to linearity issues. The peak amplifier biased in a class C, when starts operating still remains in its nonlinear region and so it is usual to see the Doherty configuration combined with other linearization techniques such as the digital predistortion. Envelop tracking also forces the introduction of linearization techniques to prevent distortion, because if the envelope tracking PA is operating in maximum efficiency mode, then it will introduce distortion that compromises the linearity of the PA.

The most common linearization techniques implies the insertion of an additional block in communication chain to compensate for PA nonlinearities and at the same time allowing operation with less back-off and therefore higher efficiency. Theoretically, the linearization can be reached modifying the signal either at input or at output, and that change can be performed exclusively in analog or digital domain.

A well-known analog technique in real communication systems is the feed-forward. This technique is quite old, proposed by H. Black in 1928, and revised later by H. Seidel in 1971 [67]. However, it is constantly integrated in real systems, mainly in base stations, due to the maturity achieved over the years. The general concept of feed-forward covers the

cancellation of the nonlinearities at the output, so the output signal is compared to input signal generating an error signal that is essentially composed by the nonlinearities introduced by PA. Posteriorly, the error signal will be linearly amplified and subtracted to the output signal, remaining at final stage a linear and amplified replica of the input signal (figure 28).

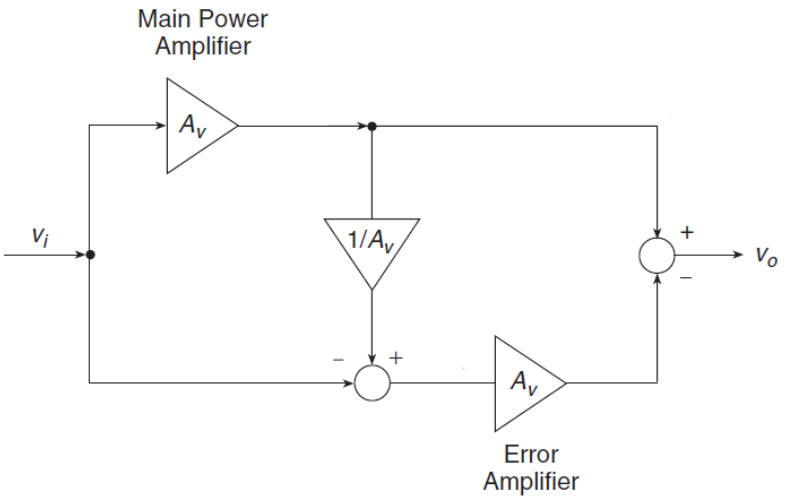

Figure 28 - Generic block diagram for the feed-forward technique (from [68])

Despite the maturity, the feed-forward has a few critical drawbacks related to the reduced overall efficiency, due to the error amplifier that must be highly linear and thus inefficient, and the need of periodic replacement of analog components because their behavior deflects according to natural aging or environment hostility, where communication system are inserted. Even more, this technique cannot accommodate a variety of standards and transmission/receive modes simultaneously, becoming an expensive and inflexible approach.

In order to solve the mentioned problems, emerge the digital techniques, as alternative more flexible and less expensive, which allow for changes at run-time of the system. Signal processing techniques can be efficiently implemented through reprogrammable hardware as Digital Signal Processors (DSPs) and/or Field Programmable Gate Arrays (FPGAs) to control the analogic RF system and also the reconfigurable hardware allows excellent reproducibility.

The linearization block including digital techniques can be placed before (digital predistortion) or after (digital postdistortion) the PA. Therefore, the digital predistortion is preferred in communication systems because its integration in system is more advantageous than postdistortion technique once the latter dissipates a non-negligible amount of power that contributes for an overall reduction of efficiency.

The digital predistortion is relatively recent, proposed by A. A. M. Saleh and J.Salz [69] in 80's. The aim involves the attempt of implementing the inverse characteristic transfer function of the PA, i.e., its role involves a transfer function that expands the signal gain to

compensate the signal compression experienced after amplification. The predistorter imposes some additional small-gain reduction to avoid the clipping of the output signal when amplified by the PA (figure 29). Theoretically, the signal obtained at the output will present better linearity properties.

In fact, it is not trivial to compute the inverse transfer function of the PA due to its mixed nonlinear and dynamic characteristics. So, the PA model requires a much more complex structure than the inverse transfer function for the predistorter (the flexibility of digital predistortion plays an important role here to implement different models of the PA).

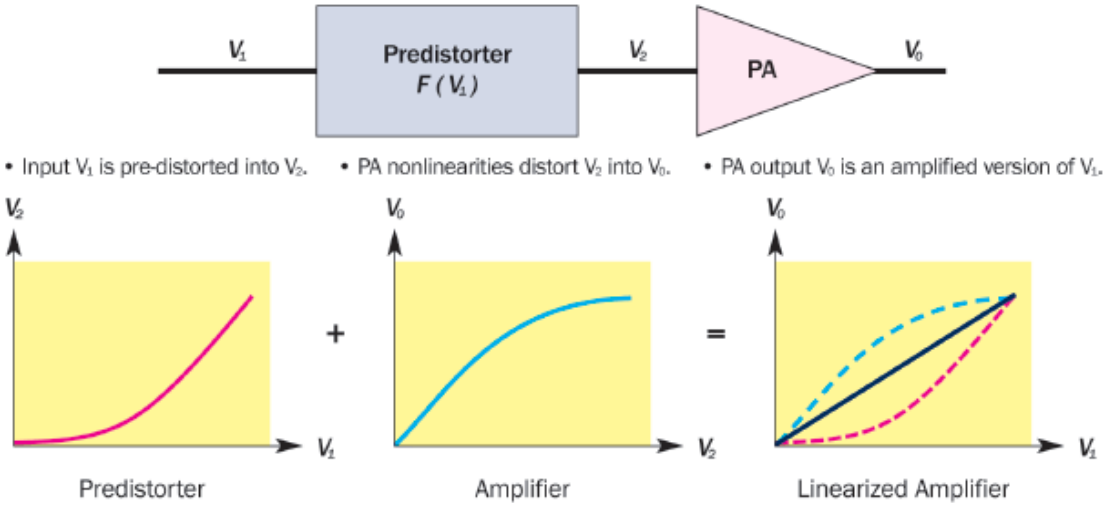

.

Figure 29 - Linearization of a PA using digital predistortion (from [70])

Several industry design experts from leading companies have reported [58] ultimate advances in implementations of each technique: Nokia/Cree/Nujira – Envelope Tracking, Freescale/NXP/Cree – Asymmetric Doherty and Xilinx – Digital Predistortion.

Figure 30 allows to evaluate the performance of the different RF PAs and linearization techniques used in communications systems over the last years, to fulfill the links requirements, following the increase on PAPR of signals. It is important to notice that the use of isolated classes AB or B based on LDMOS transistors in initial 2G generation, due mainly to their linearity, achieved 40% of average efficiency. Afterwards, their performance were considerable reduced in 3G systems, coinciding with the rise of the PAPR (3.5dB to 9dB). In fact, the employ of new modulation schemes in the recent generations, such as 3.5G and 4G, and WLAN, forced the RF PA topology to migrate to Doherty or Envelope Tracking configurations based on GaN transistors. The first combined with digital predistortion reveals 50% of efficiency and the latter performs 60% of efficiency in 4G systems which indicate a good performance when excited with high PAPR signals (8.5dB to 13 dB).

This last statement predicts the Envelope Tracking topology as the highest candidate for WPT far-field transmitters using the desired high PAPR multisine signals.

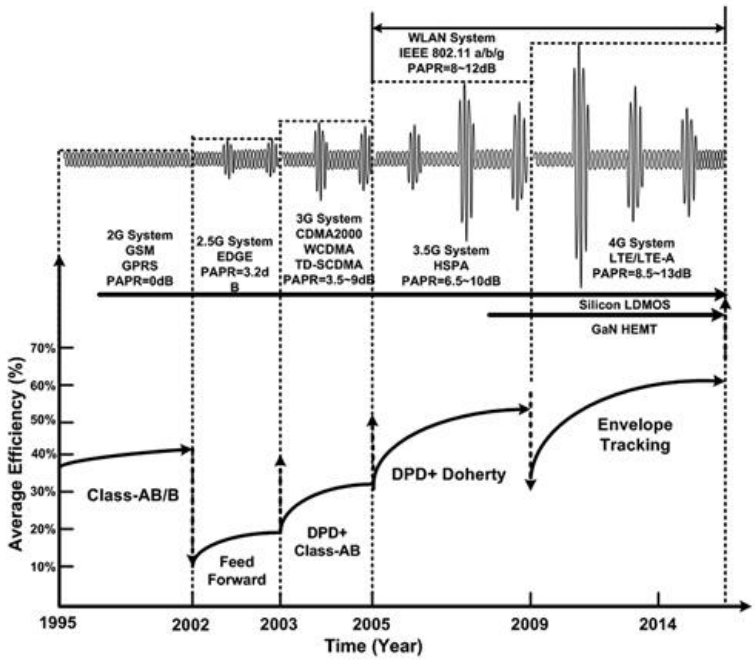

Figure 30 - The technology development of the RF PAs with the increased PAPR of signal for wireless communication standards evolution (from [58])

3. Power Amplifiers Design

In the current chapter, it will be described all the steps followed to design a PA in microstrip lines and posteriorly the details for a CPW implementation, both for a 5.8 GHz operation frequency in a class B biasing point with some harmonic control. Before that, a brief description is introduced about the chosen active device and substrate. All the simulations presented in the following sections are performed in ADS 2009 and 2011.

3.1. Active Device

The commercial diversity for discrete GaN transistors to high frequency, power and efficiency applications are rather low and after a few searches, it was verified that the GaN market is controlled by TriQuint Company. In fact, TriQuint offers GaN solutions until 18 GHz, to several output powers and efficiencies either in chip or in die. Other companies have also explored the GaN technology commercially to high frequencies, but the efficiencies reached by their transistors are lower.

The active device bought was the TGF2023-02-01, a discrete 1.25mm GaN on SiC in die, fabricated in accordance with a process named TQGaN25 exclusively from TriQuint and recently recognized as a new milestone reached on GaN reliability and heavily supported for prestigious identities as US Air Force and US Navy. This transistor is available on RichardsonRFPD and it is used mainly for wireless broadband, military and aerospace applications. The table IV shows a few important features of this device.

Table IV - Main characteristics of GaN transistor TGF2023-02-01 (from [71])

Frequency Range	DC to 18GHz
Breakdown Voltage	100V
Drain Voltage Range	Up to 40V
Gate Voltage Range	-50 to 0V
Maximum PAE (@ P3dB)	71.6%
Maximum Output Power (@ 3GHz)	38 dBm
Maximum Channel Temperature	275ºC

3.2. DC Analysis

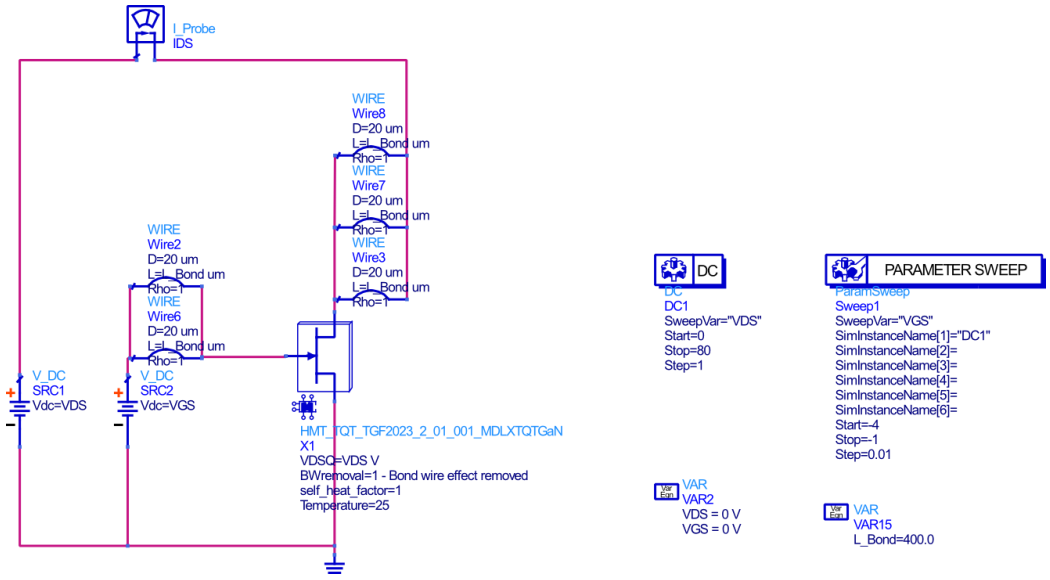

Figure 31 - Schematic used to extract the I-V characteristic curves of the transistor

Using the transistor model provided by Modelithics and the ADS schematic represented in figure 31, it is possible to trace the I-V characteristics curves of the transistor TGF2023-02-01.

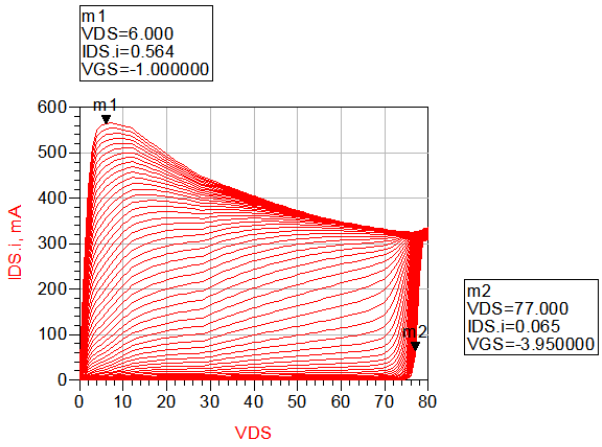

Figure 32 - I-V characteristic curves (I_{DS} versus V_{DS} for a few values of V_{GS})

The characteristics curves I_{DS} versus V_{DS} are presented in figure 32. A careful analysis points out that the transistor can provide a maximum drain current of 564 mA for a knee voltage of 6V and the breakdown voltage is approximately 80V, in contrast to the 100V indicated by Modelithics.

Although the transistor datasheet indicates a maximum V_{DS} of 40V, it is recommended to set the drain voltage to 28V to reach the maximum voltage excursion and avoid disruption. The markers m1 and m3, from figure 33 a), point out to the threshold voltage and the maximum

drain current which the transistor is able to provide. As mentioned before, the aim is a PA biased in class B, so the gate voltage was set to -2.75V, where the gm_3 (figure 33 b)) is null.

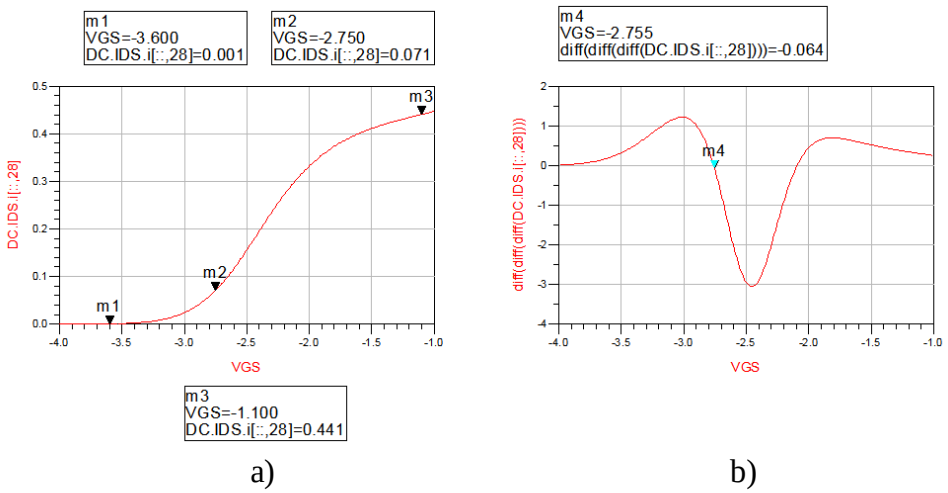

a) b)

Figure 33 - a) I-V characteristic curve for V_{DS} equals to 28V and b) gm_3

3.3. Substrate

The substrate used for the PAs design was Duroid 6010, highly recommended to high frequency RF applications such as patch antennas, PAs and LNAs integrated in satellite communications systems, aircraft collision avoidance systems and ground radar warning systems because of its high dielectric constant for circuit size reduction, tight and thickness control of the electric constant for repeatable circuit performance and lower losses until the X-band frequencies. The table V shows some important features of the used substrate.

Table V - Main characteristics for Duroid 6010 (from [72])

Substrate Height (H)	0.632mm
Conductor Thickness (T)	0.017mm
Dissipation Factor ($\tan\delta$)	0.0023
Dielectric Constant (ε_r)	10.2

3.4. Microstrip lines PA

The real active devices have intrinsic and extrinsic elements (figure 34). Either the transistor datasheet or the model available have no information about the value and behavior of these elements, so it is usual to use the load-pull technique to obtain approximated impedance

values that placed at the extrinsic drain provide more power or PAE depending on the required specifications. In figure 35, it is represented the schematic used to obtain the load-pull curves.

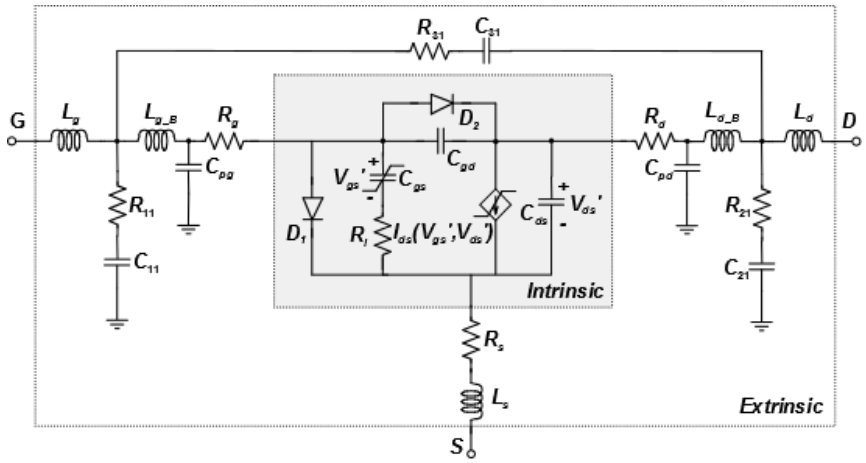

Figure 34 - Example of circuit topology for GaN modelling (from [73])

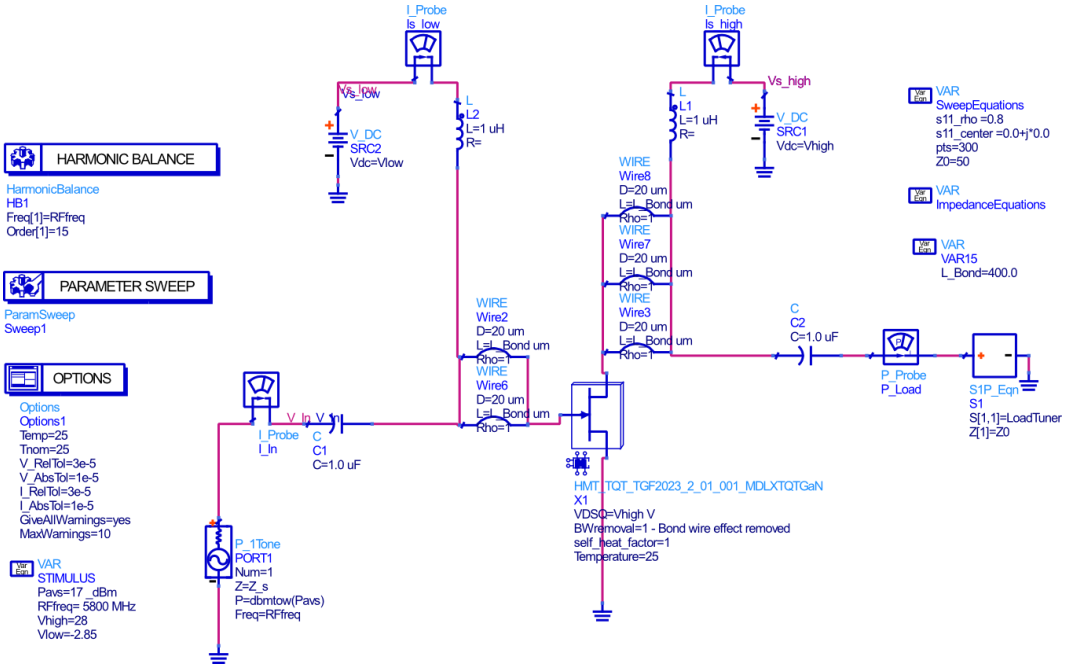

Figure 35 - Schematic used to extract load-pull curves from transistor

3.4.1. Impedances at the fundamental frequency and other harmonics

Typically, a PA is projected including a input network that allows to transform the source impedance in the impedance that the extrinsic gate must see to provide maximum transduction gain and a output network that transforms the load impedance in the impedance that the extrinsic drain must see to achieve the required output power and PAE.

The gate impedance required to achieve maximum transduction gain is extracted from a set of curves identic to load-pull curves that are named source-pull curves. Both techniques are iterative processes because the active device is bilateral and then, they only converge after a few iterations. Defined the impedances to harmonics frequencies and finished the iterative processes, the load-pull and source-pull curves are represented in figures 36 and 37.

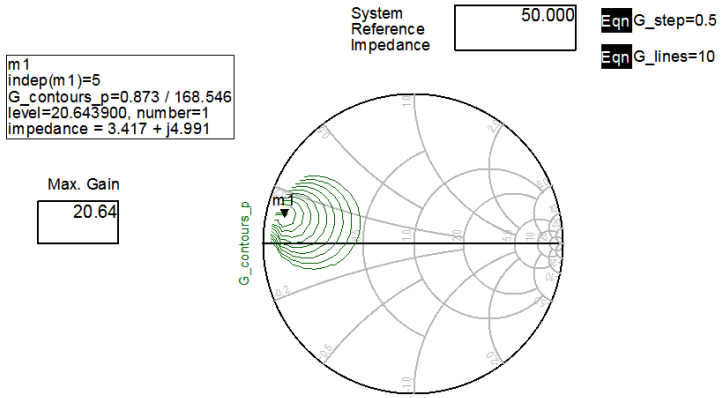

Figure 36 - Source-pull curves

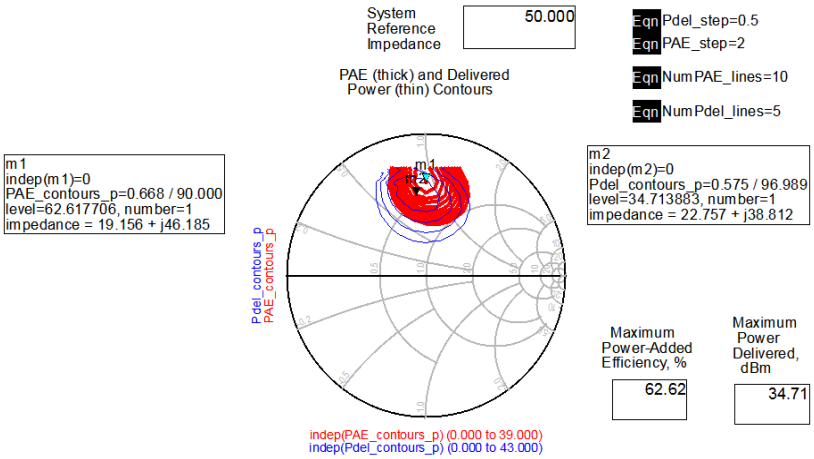

Figure 37 - Load-pull curves

According to the source-pull curves, the maximum power gain available in this class B is 20.64dB. Looking carefully to the load-pull curves, it can be obtained at 1dB compression point, 62.6% of PAE and an output power of 3W. Having in mind that the PA needs efficiency (and at least 3W of output power at 1dB compression point) and the transistor datasheet refers that the maximum PAE reachable is 71.6% at 3dB, the performance obtained above is far from the limit. Therefore, the best way to address this latter issue is try to find impedances to second (11.6GHz) and third (17.4GHz) harmonics that increase the PAE and at same time reduce the V_{GS} value (-2.85V). Thus, it was performed a load-pull to these two harmonics in order to maximize the PAE at fundamental frequency.

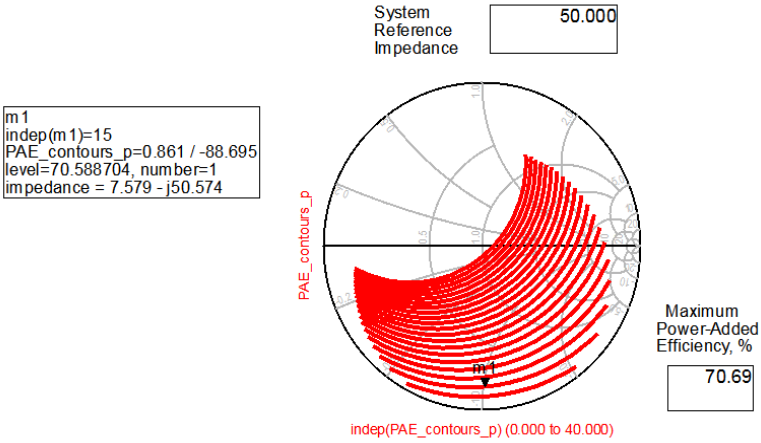

Figure 38 - Load-pull curves for second harmonic

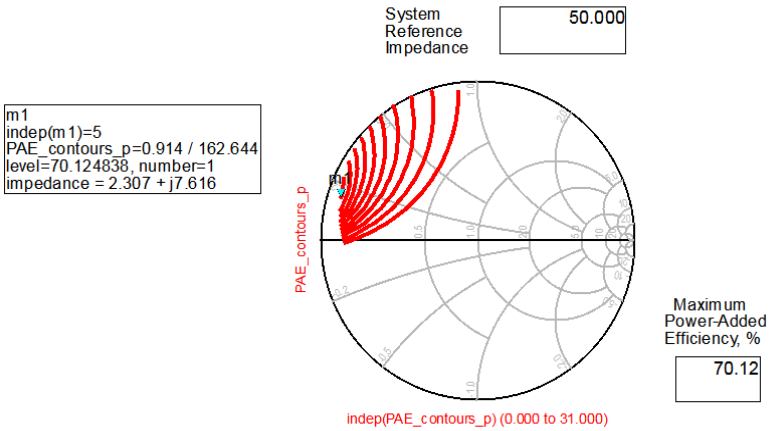

Figure 39 - Load-pull curves for third harmonic

The fourth harmonic (23.2GHz) handling was dispensed due to two reasons: the manufacturer datasheet indicates that the transistor has a maximum operation frequency of 18 GHz and the length of stub to fourth harmonic may not have a considerable length (very short) to be included in the layout.

According to the impedance values highlighted in figures 38 and 39, it was performed load-pull and source-pull again to the fundamental frequency.

In short, the impedance chosen to match the input side at fundamental frequency was 4.89 + j5.36 allowing a maximum transduction gain of 20.27dB and at the output side the impedances chosen were 19.59 + j46, 7.58 - j50.57 and 2.31 + j7.62 at fundamental, second and third harmonic respectively, performing a 71.43% of PAE and 35.08dBm at 1dB compression point (figure 40).

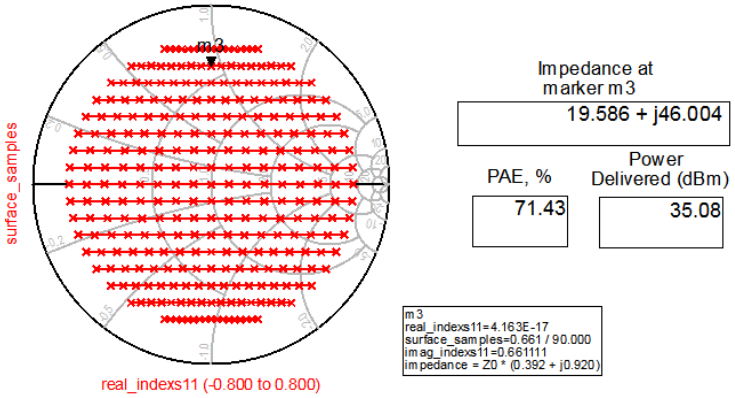

Figure 40 - Impedances mapping at fundamental frequency

3.4.2. Bias Network

The biasing network provides the necessary supply either at gate or at drain to the correct operation of the device according to the required specifications. Towards that point, the biasing network must allow that the DC component from supply source reaches the active device and prevents that RF components at fundamental frequency mixes with the DC component and vice-versa.

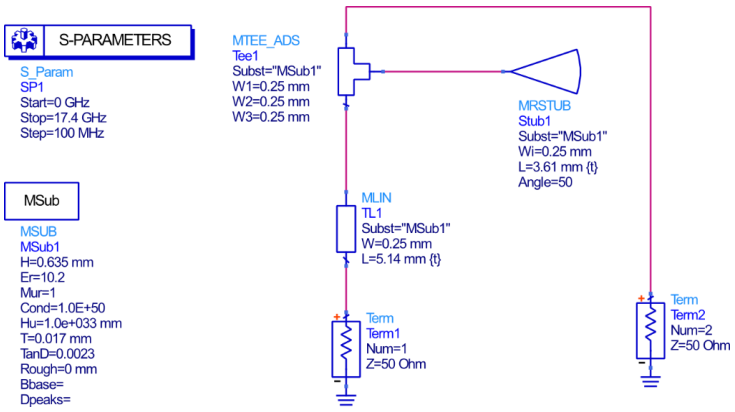

Figure 41 - Bias Network

The biasing network presented in figure 41 is constituted by a quarter-wavelength line and a radial stub. The radial stub is designed to work as a second quarter-wavelength line, performing an open circuit in its extremity and a short circuit at its center. Thus, the second quarter-wavelength line transforms the short circuit in an open circuit for the fundamental frequency. These lines must be as thin as possible in order to perform a high impedance to forces open circuit.

The radial stub could be replaced by a parallel capacitor, but for the current operation frequency, the short circuit provided by the capacitor at the end of the quarter-wavelength line may not have the necessary accuracy in a practical implementation leading, probably, to a low performance. The radial stub solves that practical problem and still increases the bandwidth where the short condition is verified.

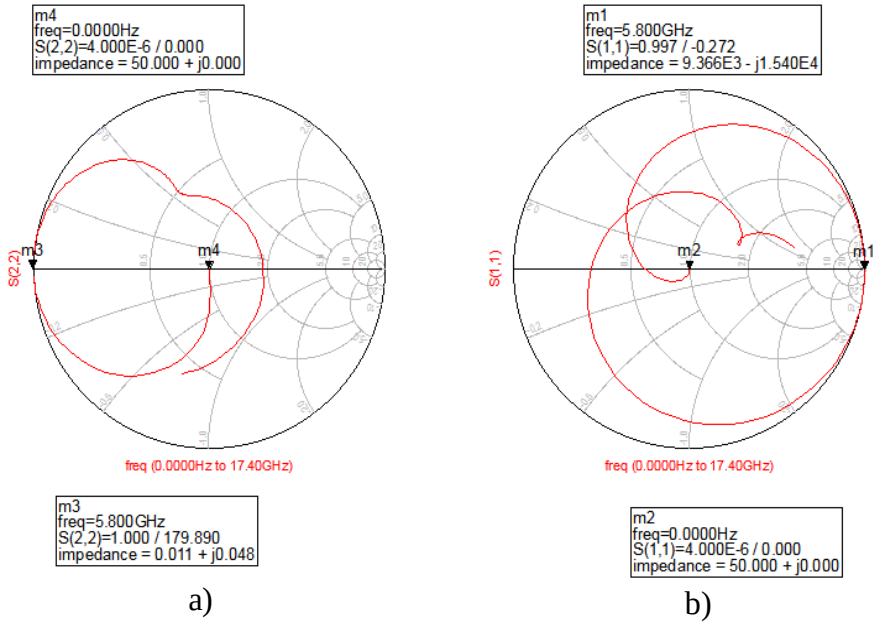

a) b)

Figure 42 - Bias Network a) S_{22} **and b)** S_{11}

The figure 42 confirms a well-designed biasing network at the fundamental frequency. The S_{11} parameter reveals an open circuit at 5.8 GHz avoiding that RF signal mixes with the DC components. On the other hand, S_{22} parameter shows a short circuit at 5.8 GHz meaning that the DC components do not mix with RF signal. To 0 Hz frequency, either S_{11} or S_{22} indicates perfect matching that allows DC supply to deliver all the power to the active device.

3.4.3. Input Network

The first version includes the biasing network to the gate, a line and stub to aim the required impedance and a DC blocking capacitor. In order to set all the correct length to each microstrip line, it is important start from an estimation of its electrical lengths to avoid physically unattainable solutions that can be obtained using directly the optimization cockpit from ADS. The initial estimation was reached resorting to a tool included in ADS named as Smith Chart. This tool sizes, with some accuracy, the electrical length of the line and stub to the fundamental frequency. Finally, the LineCalc tool converts the electrical lengths in physical lengths.

After this estimation, it can be used the optimization cockpit to achieve the lowest physical lengths possible for the line and stub. This procedure results in the network presented in figure 43 with the respective S_{22} simulation (figure 44).

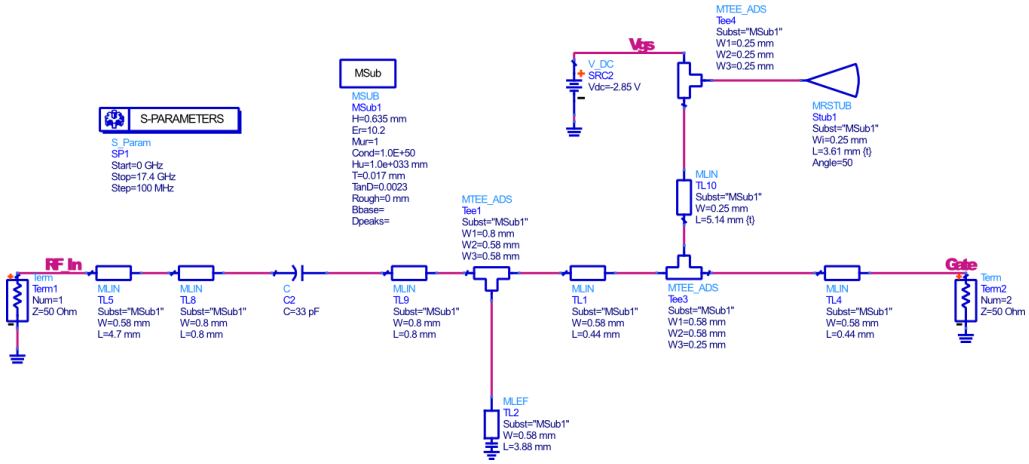

Figure 43 - Input network

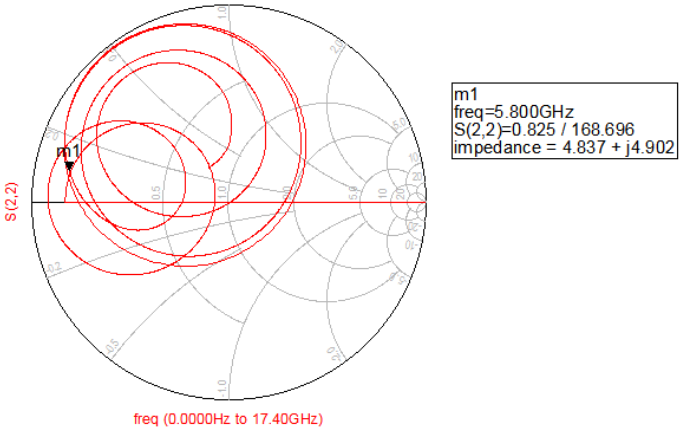

Figure 44 - Input network S_{22}

Observing the S_{22} parameter, the input network was designed to extract the maximum transduction gain from the active device.

It should be noted the presence of two lines near the DC block that simulate the capacitor pads to weld it. This procedure is very important in designs for high frequencies because the length of pads compared to the wavelength may affect the network behavior.

3.4.4. Output Network

The output network design is more complex than the input network, since additional terminations to second and third harmonics are necessary. Thus, the first step was to achieve the impedance for the fundamental frequency using the same procedure described in the input network. For the second and third harmonic, it could be adopted a similar strategy to dimension

the length of lines and stubs to get the desired impedance. However, the conductor losses will be more significant with the increase of lines placed in the RF signal path. So, the approach taken includes one more line and stub to match the second and third harmonic impedances (figure 45).

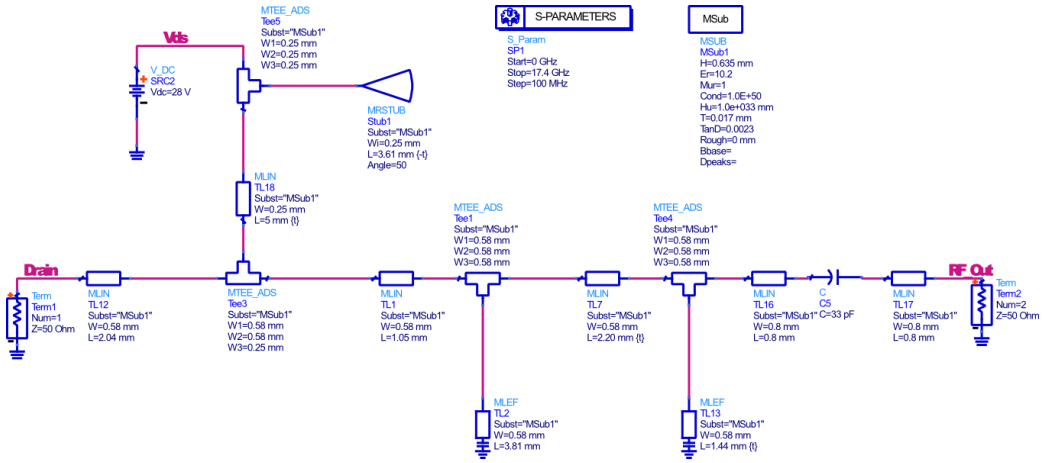

Figure 45 - Output network

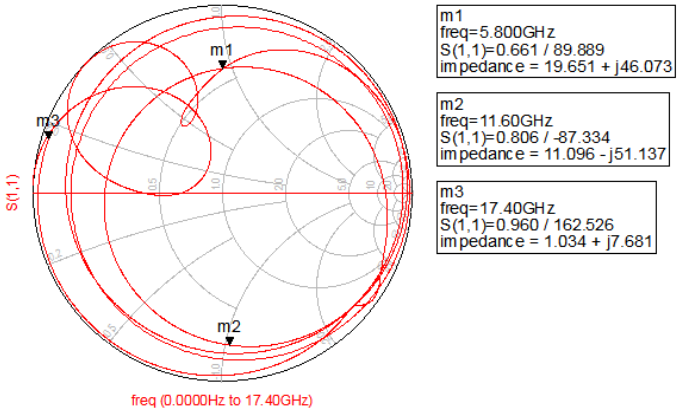

Figure 46 - Output network S_{11}

Observing figure 46, the projected output network presents all the impedances mentioned before.

3.4.5. Stability

After the conclusion of the input, output and biasing networks, it is absolutely important to proceed to stability analysis of the PA. ADS has a tool that traces automatically the stability circles for several frequencies and indicates which regions inside the Smith Chart are stable resorting to a basic S-parameter simulation and theoretical concepts mentioned in Chapter II.

Starting with a small-signal analysis to evaluate the PA stability for all operation frequencies, it was verified that for a short range of frequencies below the fundamental frequency, the PA was potentially unstable at source side. That problem was solved by inserting a 4.7Ω resistor in the biasing network placed at input network. So, the input network was dimensioned again.

The figures 47 a) and b) show the stability results after the insertion of the 4.7Ω resistor, showing the stability circles for 0 Hz until 18 GHz with a step of 25 MHz either at input or at output side. The 50Ω load (blue point) is always in stable region for all situations.

However, as the designed PA can be operating in saturation regions for the purpose of power transfer in WPT applications, it is important to perform a large-signal analysis to verify the stability of the PA in those regions. Towards that point, ADS has also a tool that allows the stability analysis under large-signal operation. So, fixing the operation frequency to 5.8GHz, it was made a sweep in input power from -40dBm until 25dBm and plotted the results in figures 47 c) and d). The 50Ω load (blue point) is always in stable region for all situations.

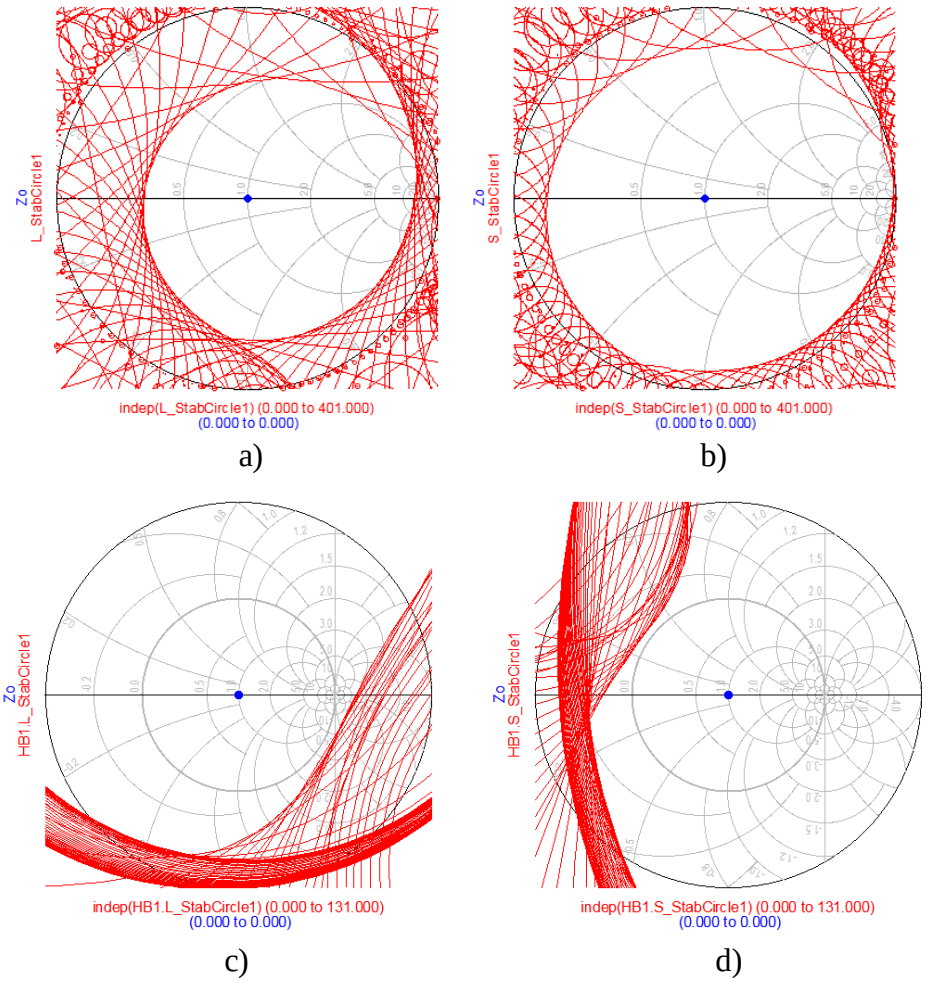

Figure 47 - Stability circles for small-signal a) load and b) source and large-signal c) load and d) source

3.4.6. Final remarks in microstrip PA

A few adjustments were performed in the two networks (figure 48 and 49) to achieve the final layout. 50Ω lines were inserted both at the input and at the output side to weld the surface mounted device (SMD) connectors for RF signal and adjust the circuit to the produced brass box. On the other hand, the quarter-wavelength lines in biasing network were curved to reduce the circuit size. At last, ground planes were inserted to weld the DC filtering capacitors.

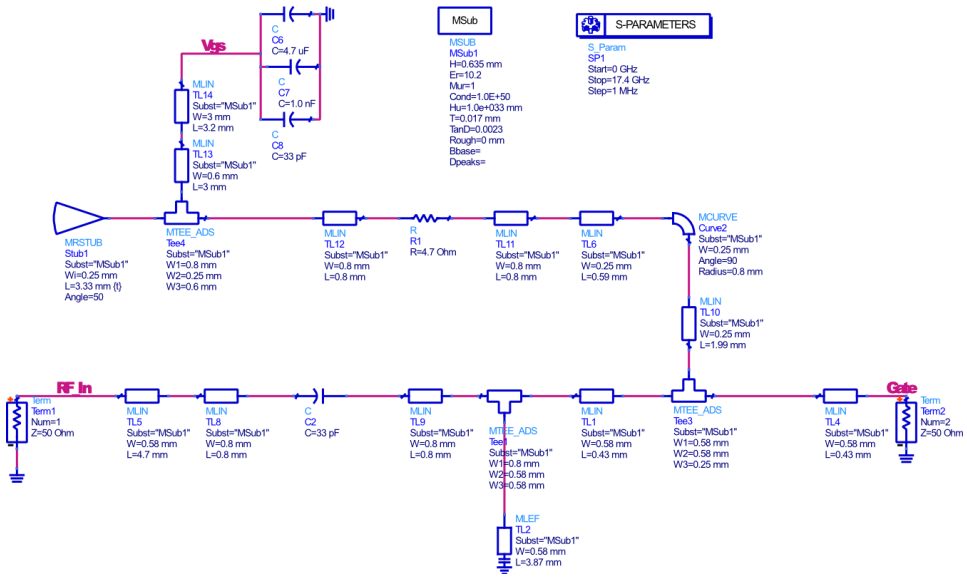

Figure 48 - Final input network

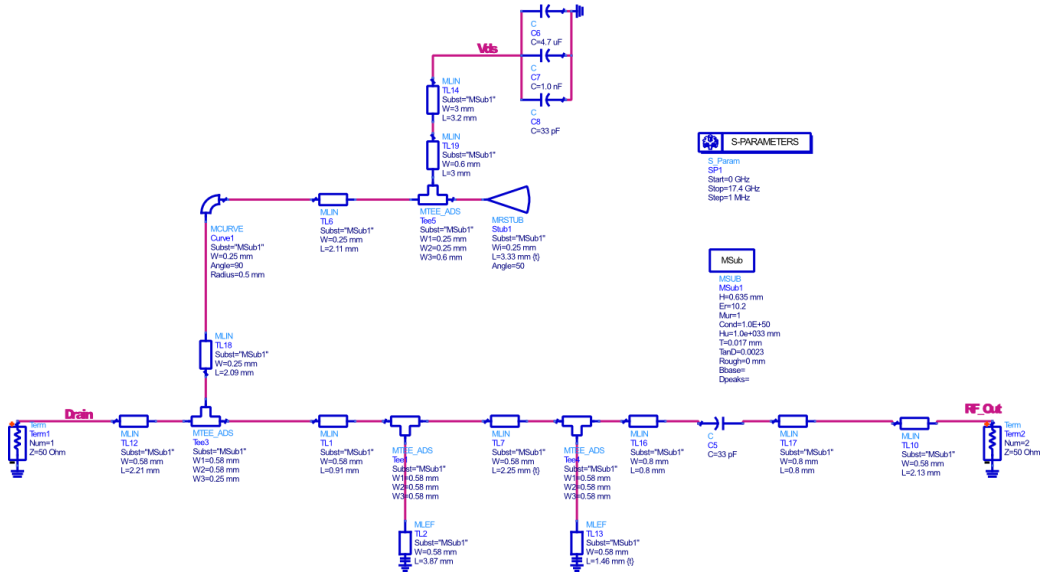

Figure 49 - Final output network

3.4.7. Figures of merit

After guaranteeing the small-signal and the large-signal stability, it was performed a 1-tone harmonic balance (HB) simulation to evaluate the PA performance at 1dB compression point. The table VI resumes the information from figure 50.

Table VI - Figures of Merit for the microstrip lines implementation

P_{in} (dBm)	PAE (%)	η (%)	Small-signal gain (dB)	P_{out} (dBm)
17.5	70.8%	71.8	18.6	35.1

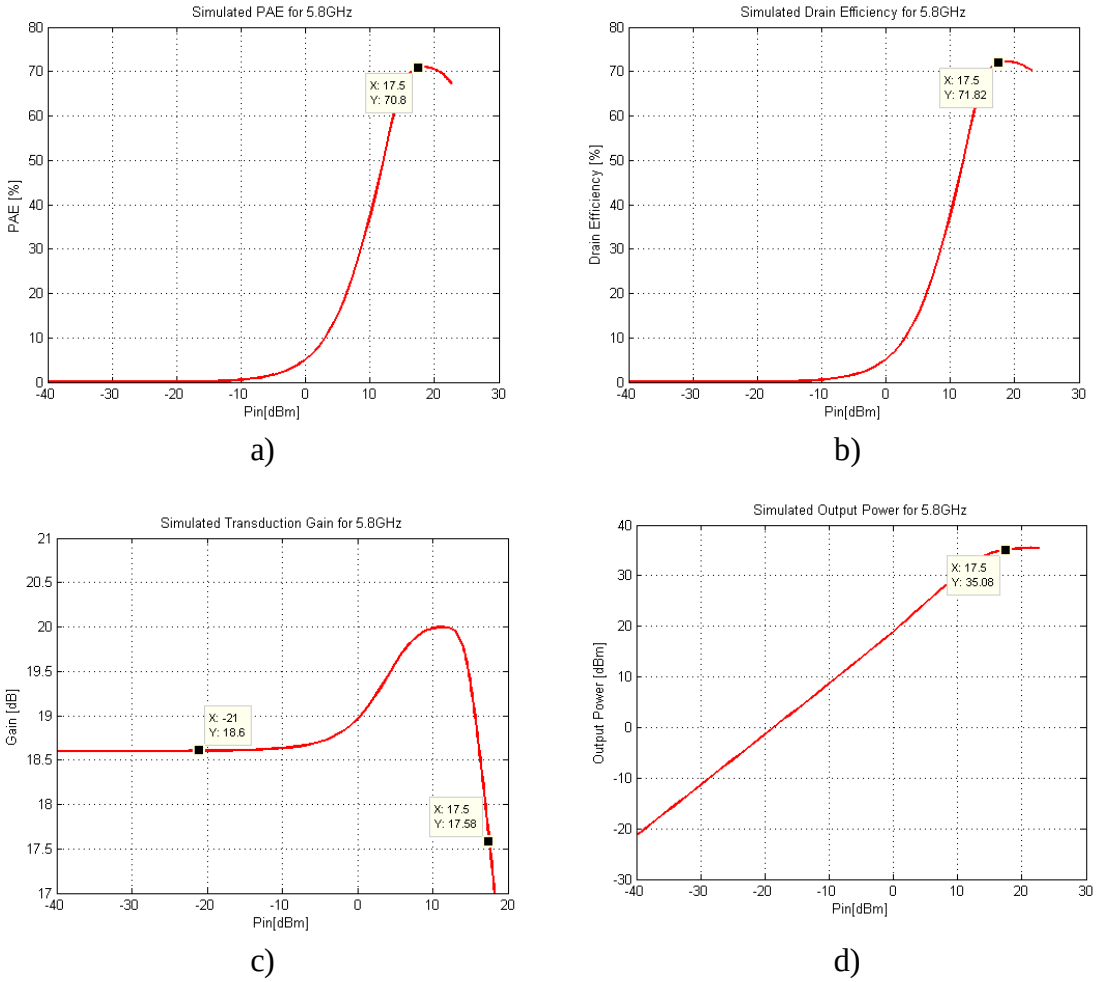

Figure 50 - Figures of Merit for the microstrip lines PA a) PAE, b) η c) gain and d) output power

3.5. Coplanar Waveguides PA

3.5.1. Planar Transmission Lines

The planar transmission lines are a basic element in MMIC design and then they are often used in several RF applications such as filters, couplers, power dividers, tuning stubs, matching networks and connecting antennas to the rest of the RF system. Thus, MMIC has an important support to occupy a prominent place in actual RF systems due to the reduced size of produced circuits, lighter designs, electrically efficient and an affordable cost of production [74]. In addition, the nature of the active devices to modern microwave applications as diodes or transistors based on GaN or GaAs have stimulated even more the development of structural techniques that allows the integration of these devices in MMIC.

Typically, the planar transmission lines consist of strips of metallic conductor placed over a substrate and they can be named differently according to the design structure adopted:

A. Microstrip lines

Microstrip lines deserve a special highlight because they are massively used in current design of MMIC for RF systems. The microstrip lines are constituted by a single conductor trace on one side of the dielectric substrate and a single ground plane on other side (figure 51).

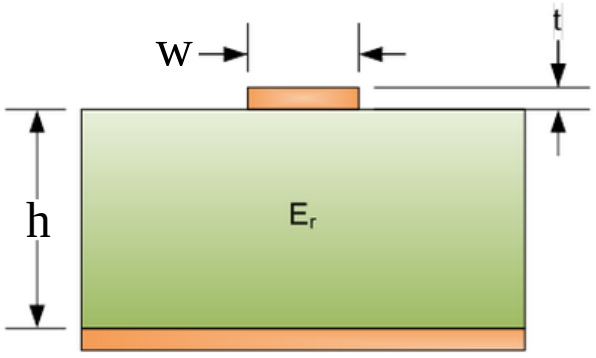

Figure 51 - Cross-sectional view of a microstrip line (from [75])

The microstrip lines are open structures and then, its production process is relatively relaxed and allows ease interconnection and adjustment. However, the microstrip lines have also important limitations, essentially to high frequency applications.

The fundamental propagation mode in microstrip lines is quasi-TEM and has a 0 Hz cut-off frequency. A quasi-TEM mode is highly dispersive to high frequencies because the

electromagnetic field is more and more concentrated into the substrate material [76]. This means that the propagation velocity will vary significantly when the frequency increases, resulting in characteristic impedance and dielectric effective constant variations. On the other hand, as microstrip lines are involved by air, when the frequency rises, they tend to act as antennas. This behavior leads to energy loss in fundamental mode that are called radiation losses. The use of microstrip lines is fully centered to frequencies where these phenomena are neglected.

B. Coplanar Waveguides

With the growth sensed in high frequency applications in recent years, a large investment was made to develop the CPW technology in order to strengthen its position in MMIC design because the CPW has advantageous characteristics related to microstrip lines. The concept of CPW was initially suggested by C. P. Wen in 1969 [77] as an alternative to design microwave circuits to high frequencies. A conventional CPW fabricated using a substrate involves a central conductor trace surrounded by ground planes at equal distances from it (figure 52).

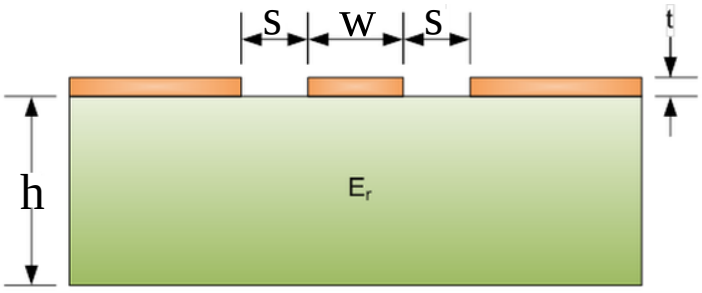

Figure 52 - Cross-sectional view of a typical CPW (from [75])

As the three conductor parts are in the same reference plane, the CPW originates two fundamental modes with cut-off frequencies equal to 0 Hz: the even mode (coplanar waveguide mode) which has equal potentials to the ground planes and the odd mode which has ground potentials of different signals but equal magnitude;

The CPW concept was defended again in 1976 and 1977 by M. Houdart [78], highlighting the good properties. For instance, placing series or parallel components is much easier. In case of parallel components, there is no need to make vias until the ground plane placed under the substrate as happens in microstrip lines. As consequence, the connections until the ground plane are more reliable and the circuit design is more compact because there is no need to allocate space for the vias and this procedure avoids parasitic inductances.

The fundamental even mode is a quasi-TEM mode and its dispersion is lower (figure 53 and 54) than in microstrip lines. For this reason, the fundamental mode is pleasant for broadband applications. On the other hand, the odd mode suffers the same drawback as microstrip lines related to the dispersion issue.

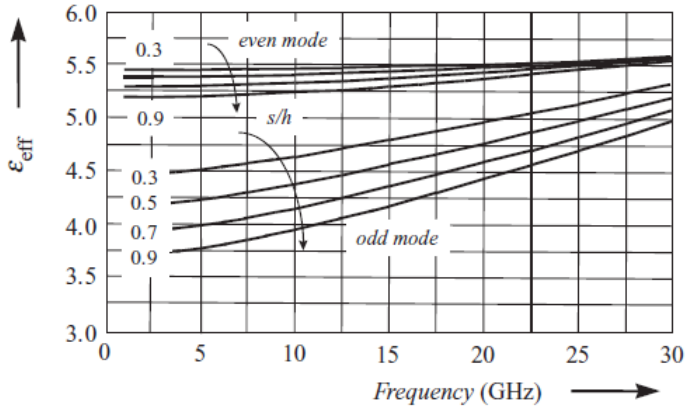

Figure 53 - Frequency dependence of the effective dielectric constant of the even and the odd mode on CPW (from [76])

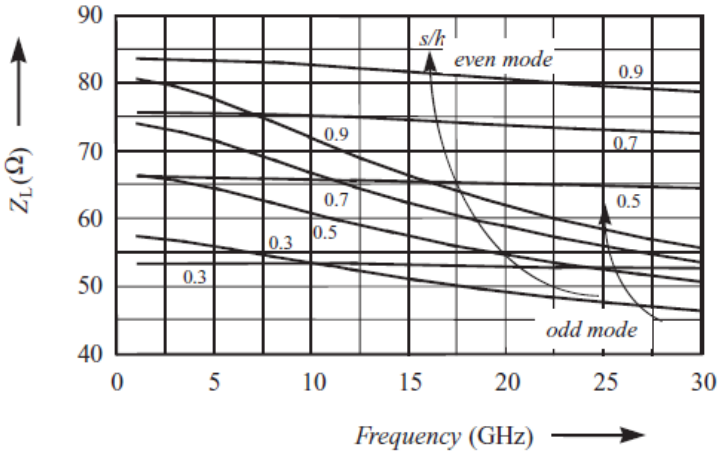

Figure 54 - Frequency dependence of the characteristic line impedance of the even and the odd mode on a CPW (from [76])

The CPWs provides better isolation between the traces due to the presence of the ground planes acting as shields and the impedance characteristic has a wide range variation caused by the low influence inflected by the substrate thickness on it.

Although the several advantages presented, this technology have failed the replacement of microstrip lines in MMIC design, because the microstrip lines are a well characterized component due to the extensive utilization over the years, providing a reliable design. The CPW still needs accurate models to high frequencies to reverse the MMIC design paradigm. In fact, the analysis methods for quasi-TEM mode in CPW find several approximations and it is often performed over empiric results [79]. The CAD tools available (for example AWR and ADS) have libraries directed to CPW but they are very limited, especially when the components are

discontinuities (for example coplanar open end, short circuit end, bend, t junction and air bridges).

The CPW lines have also some disadvantages that cannot be neglected and require careful attention from the designer. The conductor losses on CPW lines concerning to even fundamental mode are higher than in microstrip lines (then the attenuation is higher too), because the electromagnetic field is so closely concentrated in the gaps between the conductors that the current inside the center strip and the ground planes is heavily concentrated near the edges of the conductors increasing the losses. This effect is even more pronounced when the gap value decreases (figure 55).

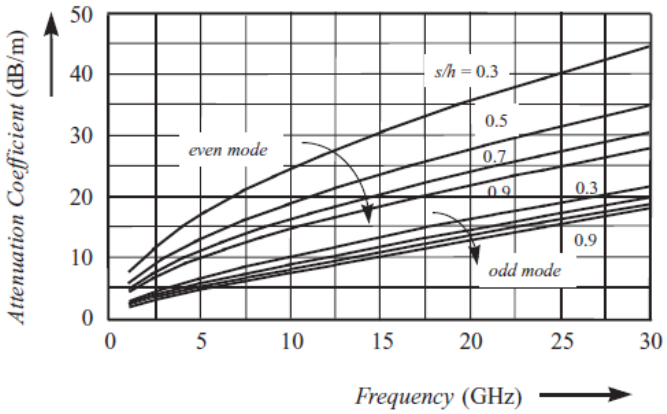

Figure 55 - The frequency dependence of the attenuation coefficient of the even and the odd mode on a CPW (from [76])

The CPW lines suffer from multimode propagation. In order to suppress the odd mode, the procedure commonly followed is the use of air bridges that allow to maintain the ground planes at the same potential. For higher order modes until the last frequency of interest in circuit operation, some authors suggest that it is necessary to keep the dimension $w+2s$ less than 45^{o} long than the highest frequency of interest [80], while others defend that it is indispensable to confirm through a several tests (trial and error procedure) that the chosen dimension fulfills the desired compromise, lower losses and absence of multimode propagation.

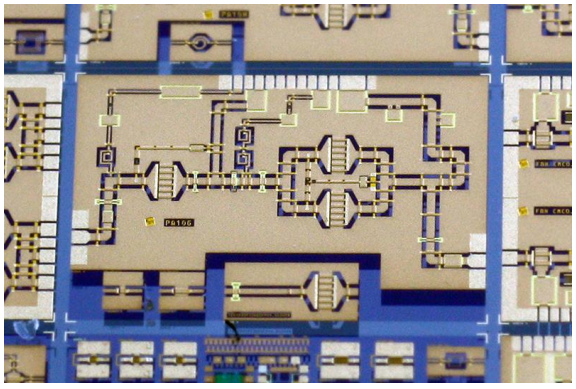

Figure 56 - FBH X-band PA in a CPW implementation (from [81])

The CPW lines are already used in several RF applications such as PAs (figure 56) and Low Noise Amplifiers (LNAs) in order to check its performance and aim a gradual trend to replace the microstrip lines to high frequency applications [81].

3.5.2. CPW implementation

The CPW PA uses the same impedances that were showed in microstrip design. However, as mentioned, the CPW design reveals more complexity than microstrip design due to the scarce characterization of CPW lines in CAD programs. The libraries available on CAD programs are very limited. For instance, the library available on ADS to CPW does not provide discontinuities such as bends and t junctions.

The t junctions are discontinuities used to join lines with different propagation properties and so, they are very influents in PA performance. The absence of t junctions in simulations and measurements at low frequencies can be irrelevant, but when the frequency increases, the addition of any element to join the lines without simulate its behavior can be disastrous. In face of this situation, there are two exit scenarios: the first scenario is try to find another CAD program more evolved in CPW field. The AWR is a similar program to ADS and has also a CPW library. Although there are components that are not available on ADS as t junctions, they exist in an open form, i.e., they are only characterized for a predefined W and S parameters. If the W and S change their value, the AWR needs to simulate the behavior of the component to the desired frequency and dimensions chosen. This simulation is extremely slow and cannot reach credible results.

The second scenario is to try to build a t junction in a layout tool, simulate its S-parameters and import that values to a black box that will replace the conventional t junction in schematics. The goal is not to provide an exact technical solution but a solution with an acceptable behavior for the fundamental frequency that minimizes the design error in CPW lines.

3.5.3. T junction simulation

Before starting the process of developing a CPW t junction, it is important having in mind the importance of transversal section dimensions in CPW to fulfill a compromise between attenuation and multimode propagation. Thus, complying the condition suggested before, that referred the cross-sectional could not exceed 45º long than the highest frequency of interest, a few pairs of values for W and S dimensions were tested in LineCalc tool to discover which ones fulfill the condition. So, the maximum values for W and S dimensions that satisfy the condition

are 0.24mm and 0.15mm, respectively. Due to technical limitations these dimensions cannot be performed. So, the next approach considered to get feasible dimensions was to set S=0.3mm and W=0.39mm to give some margin in boards production.

Afterwards, it was used the layout tool of ADS to design the t junction with the respective dimensions. The designed t junction does not respect the conventional structure of CPW lines, i.e., ground planes equidistant to a central conductor trace above a substrate with finite thickness. As there are not technical conditions to include air bridges that connect the two ground planes to maintain them at the same potential, it was opted by other usual structure that includes a ground plane below the substrate, conductor backed coplanar waveguide (CBPW).

The t junction with 50Ω branches has the appearance showed in figure 57 a) and the respective S-parameters simulation is in figure 57 b).

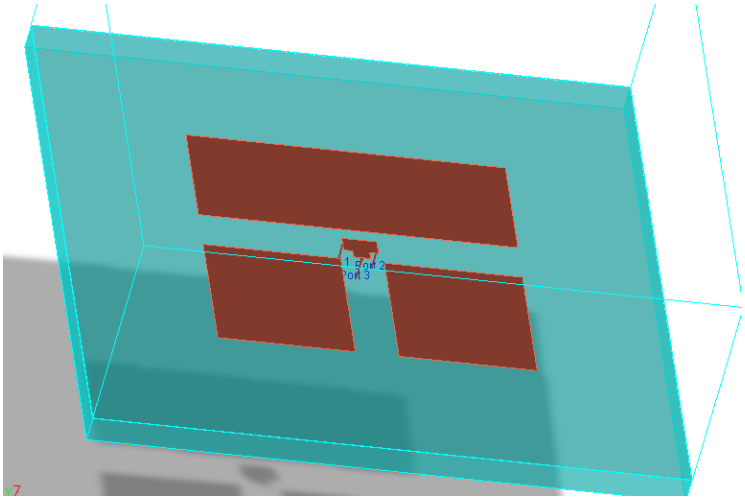

a)

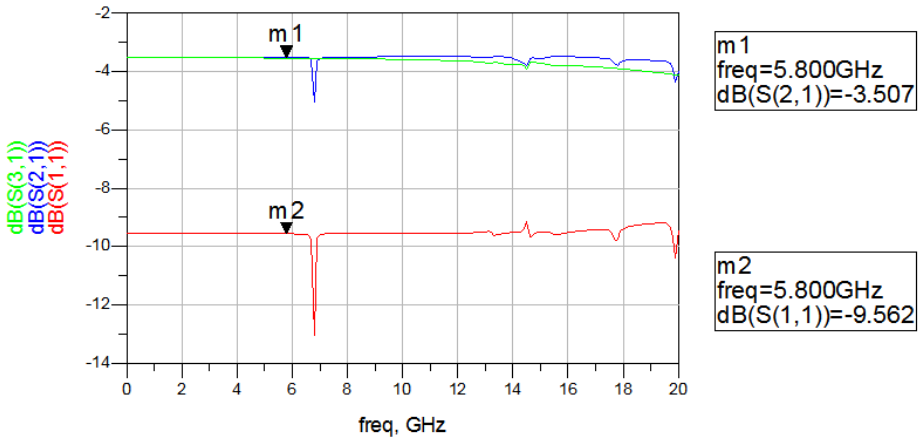

b)

Figure 57 - a) Three dimensional view of the designed t junction on CPW and b) respective S-parameters simulation

The t junction designed acts as a power divider until nearly 10 GHz. So, it can be used for designs at 5.8 GHz.

3.5.4. Networks design

The project of each network includes every step taken in microstrip section. In the input network (figure 58), the impedance reached was the same that provides maximum transduction gain (figure 60). On the other hand, as it can be seen in figure 61, the impedances of the output network (figure 59) are different, but they were chosen to maintain a similar performance.

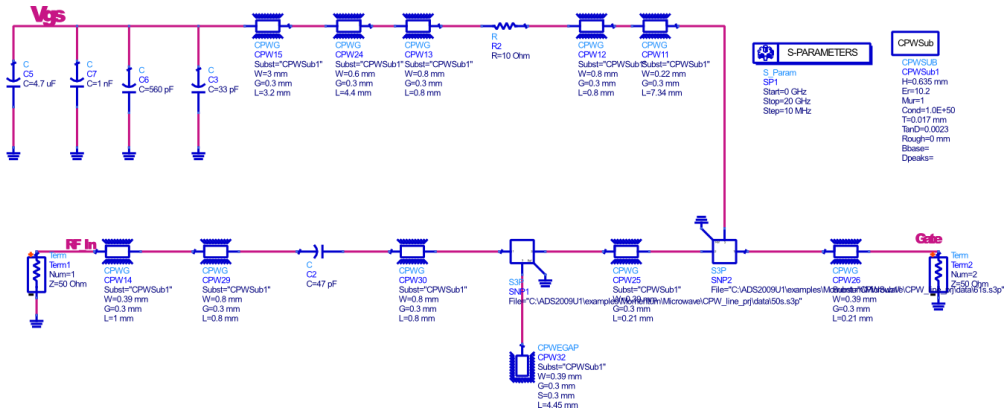

Figure 58 - Input network circuit

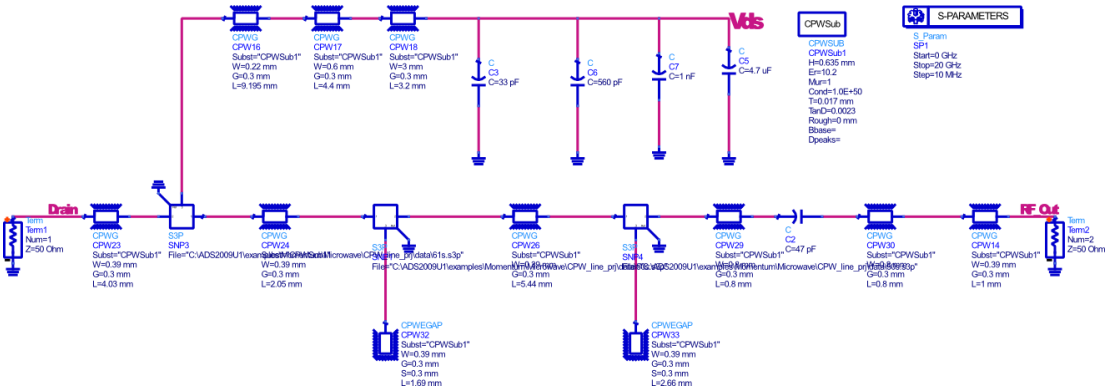

Figure 59 - Output network circuit

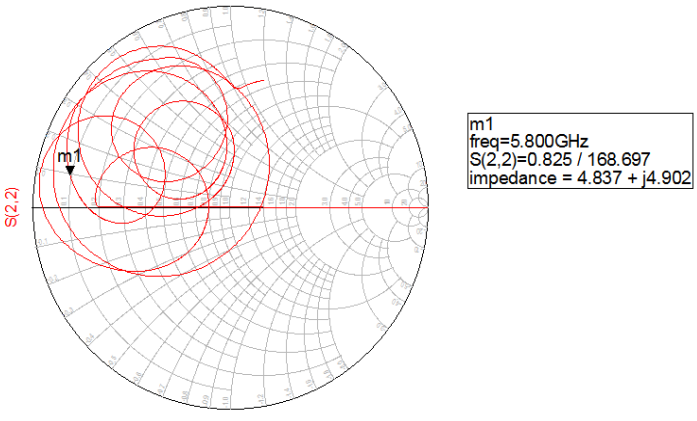

Figure 60 - Input network S_{22}

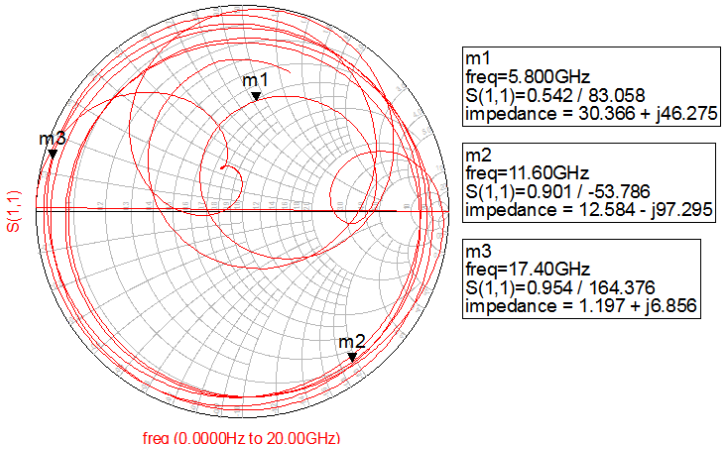

Figure 61 - Output network S_{11}

3.5.5. Stability

As it happens in microstrip lines implementation, it was performed a few modifications in the networks in order to integrate SMD connectors and DC filtering capacitors. A resistor of 10Ω was introduced in the gate biasing network to guarantee the PA stability for small-signal and large-signal (figure 62). After that, the 50Ω load (blue point) is always in stable region for all situations.

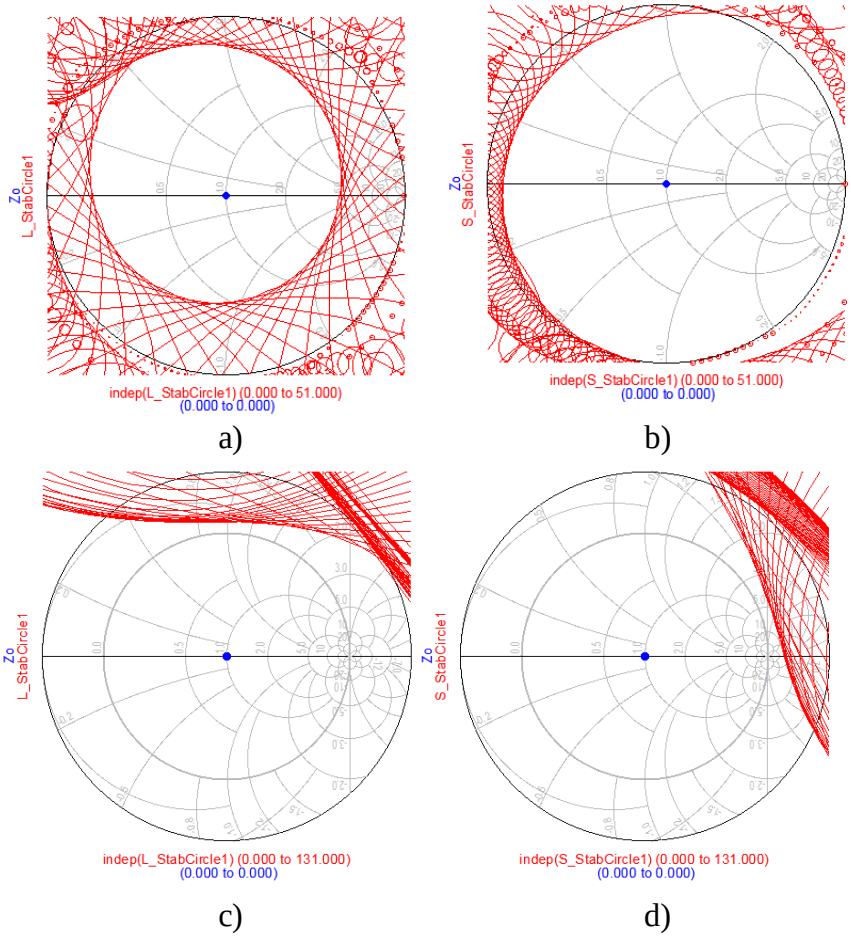

Figure 62 - Stability circles for small-signal a) load and b) source and large-signal c) load and d) source

3.5.6. Figures of merit

After guaranteeing the PA stability, it was performed a 1-tone HB simulation to evaluate the PA performance at 1 dB compression point. In figure 63 are presented the results for that simulation and the table VII resumes that information.

Table VII - Figures of Merit for the CPW implementation

P_{in} (dBm)	PAE (%)	η (%)	Gain (dB)	P_{out} (dBm)
18.8	69.3%	70.5	18.2	36.1

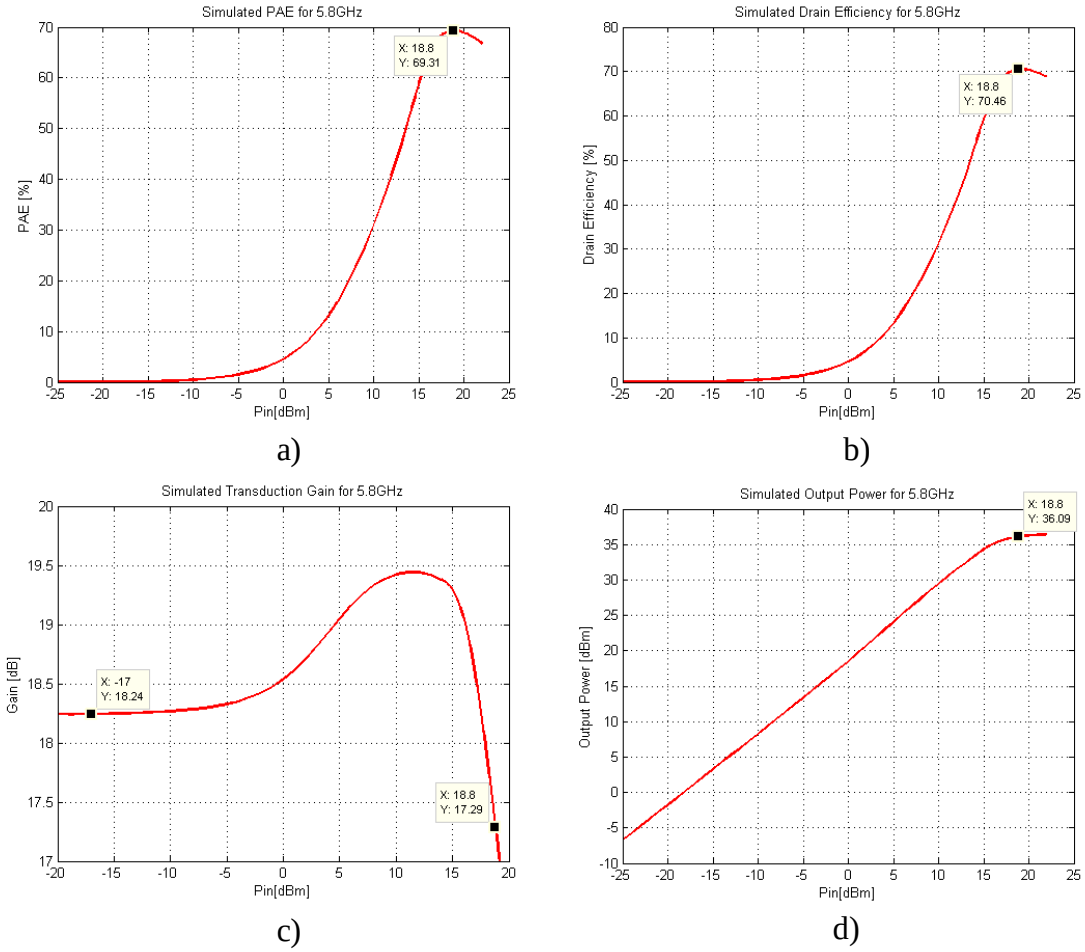

Figure 63 - Figures of merit for coplanar waveguides PA a) PAE, b) η , c) gain and d) output power

As expected the PAE (and drain efficiency) obtained is lower than in microstrip implementation due to the new impedance at fundamental frequency. In contrast, the output power is higher, achieving near to 4W at 1 dB compression point.

4. Implementations and results

In this section are shown the layouts designed to each PA. Both PAs were produced in order to compare, under the same biasing point and requirements, the practical performance for each transmission line implementation. For that purpose, S-parameters, continuous wave (CW), 2-tone and modulation tests were performed to evaluate the microstrip PA.

4.1. Layouts and some notes about the boards

The circuit board for the microstrip PA has 23.6 x 18 mm, while the CPW board has 27 x 30 mm (figure 64). The width of the CPW board is considerably larger due to the quarter-wavelength lines being not curved (absence of bends in CPW libraries of ADS).

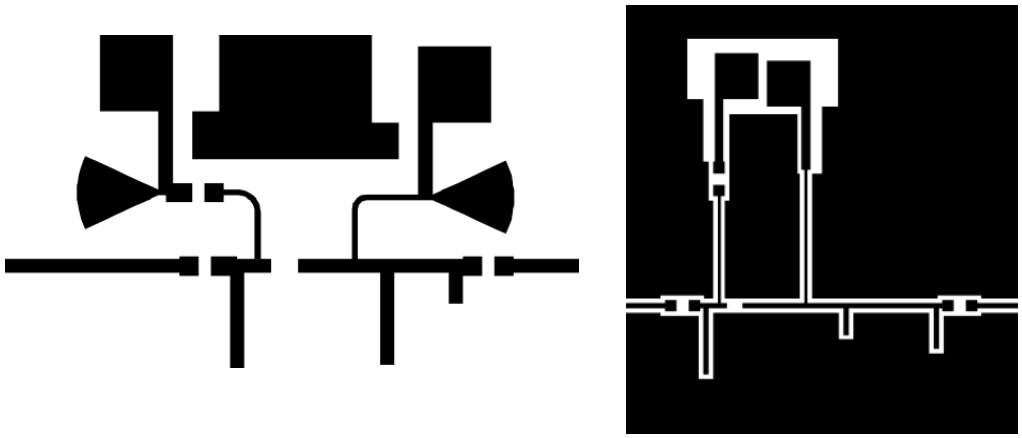

a) b)

Figure 64 - Layouts a) Microstrip and b) CPW

As the transistor is in die, it was necessary to perform bonding (figure 65) to connect the gate and the drain to the rest of the circuit board. The source did not need bonding because it is under the transistor and then, there is direct contact with the ground plane included at the bottom of the circuit board.

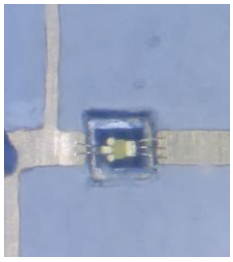

Figure 65 - Bondings in gate and drain of the transistor

Still in the production process, the two circuits were packaged in a brass box that acts as support but also as heat sink. In each design, the 50Ω lines placed at input and output sides were adjusted to achieve feasible dimensions in order to the brass box could incorporate the necessary vias for connections. The final aspect of microstrip and CPW implementations are showed in figure 66.

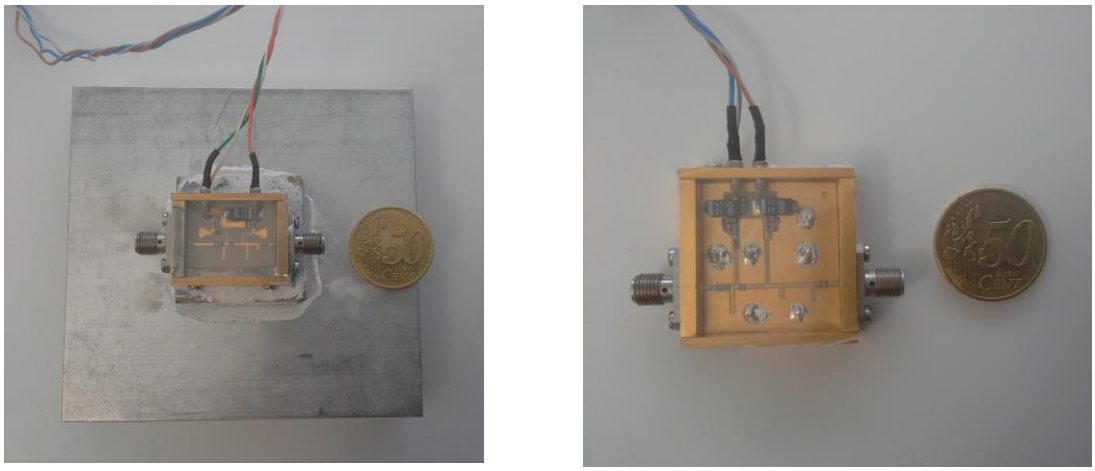

a) b)

Figure 66 - Boards a) Microstrip and b) CPW

It is important to highlight that it was also included for precaution, due to the reduced circuit dimensions, one heat sink and thermal compound to improve the heat flow from PA operation.

4.2. Measurements

Before the CW, 2-tones and modulation tests, the PAs were submitted to an S-parameters analysis, using the network analyzer E8361C from the Agilent Technologies, in order to check oscillations, transduction gain and the matching for 5.8GHz.

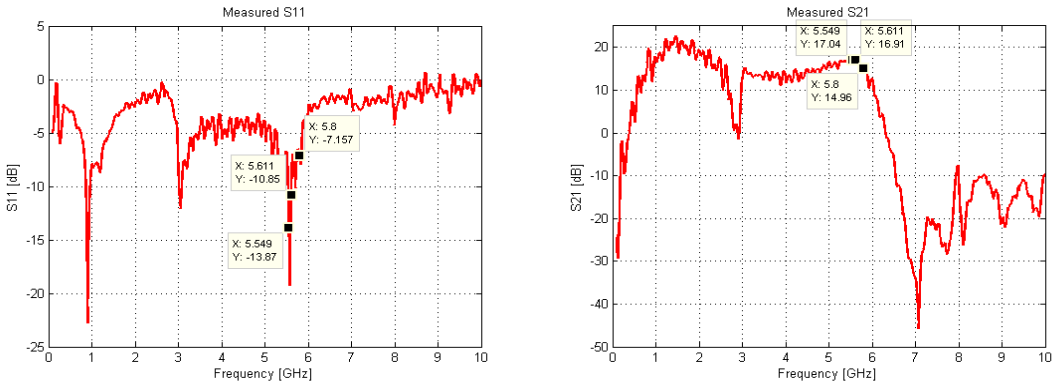

a) b)

Figure 67 - Measured a) S_{11} and b) S_{21} for the microstrip PA

The figure 67 reveals a large bandwidth for the microstrip PA, approximately 5GHz (however includes a small notch frequency close to 3GHz). The maximum transduction gain (17dB) was found at 5.549GHz, but this value is far from the small-signal gain simulated for 5.8GHz (18.6dB). In addition, the matching is also better at 5.549GHz (-13.9dB).

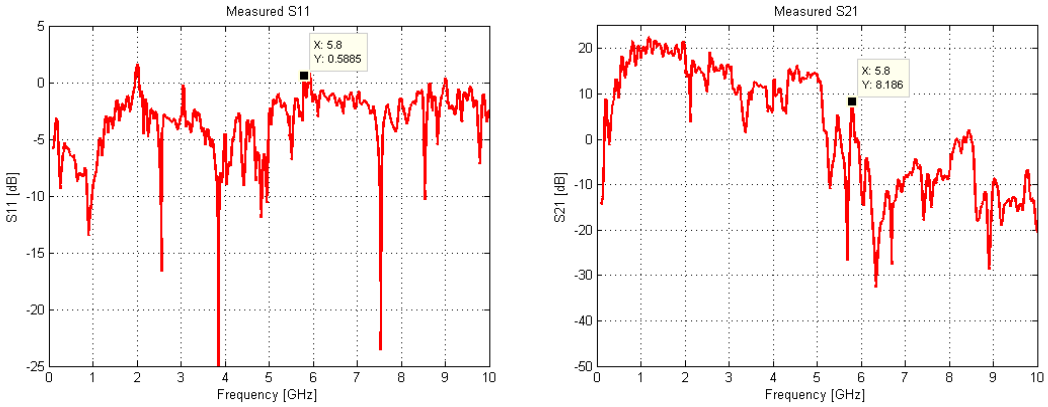

a) b)

Figure 68 - Measured a) S_{11} and b) S_{21} for the CPW PA

As it was predicted, the PA designed in CPW hardly would reach a similar performance to the microstrip PA, due to the lack of characterization of the CPW library. Thus, poor matching and low transduction gain at 5.8GHz and a few small evidences of oscillation can be seen in figure 68 a). No tests were performed to that PA.

However, it would be interesting to remove the transistor and replace it by a capacitor to perform another S-parameters analysis in order to compare how far the behavior simulated in ADS is from the practical implementation.

4.2.1. The CW measurements

The CW measurements performed with the microstrip PA used the setup represented by the illustrative block diagram of figure 69.

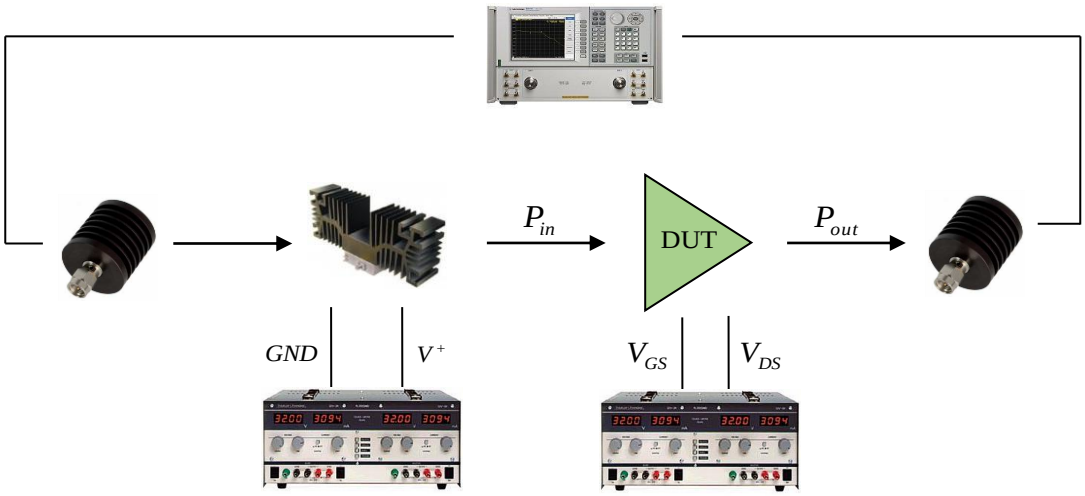

Figure 69 - Illustrative setup for CW measurements

In order to perform the CW tests, it was needed a network analyzer that allows to characterize the AM-AM and AM-PM curves with good precision.

Besides the GaN PA, device under test (DUT), it was also included a driver preceded by an attenuator of 10dB because the power levels at the output of the network analyzer are insufficient to the correct characterization of the DUT. The driver used is ZVE-8G+ of Mini-Circuits. After the DUT, there are another two attenuators, which combined are a 20dB attenuator, to reduce the power level at the input of the network analyzer to not saturate or damage its input stage. The figure 70 shows a photo of the real setup used.

Figure 70 - Real setup for CW measurements

The results obtained for transduction gain, AM-AM, PAE, drain efficiency for the highlighted frequencies in microstrip PA, are presented in figure 71.

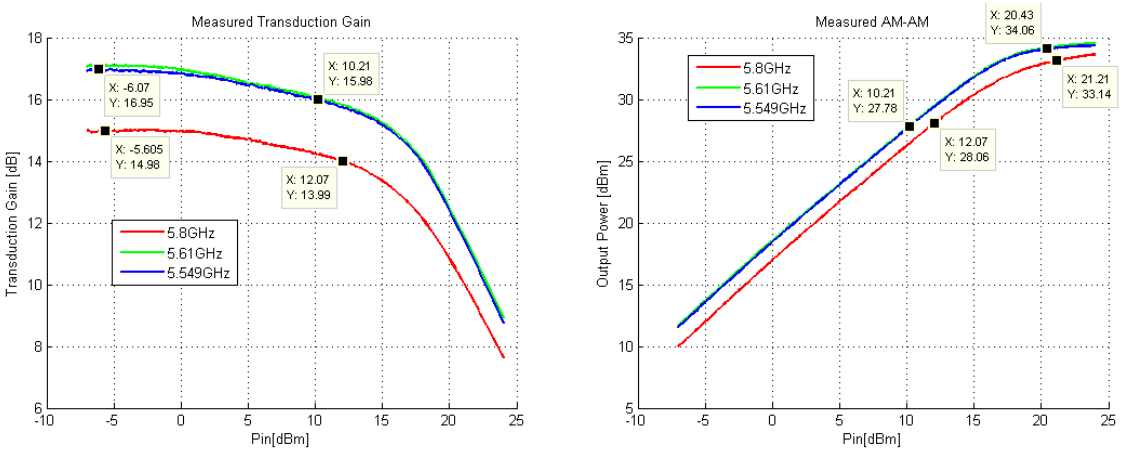

a) b)

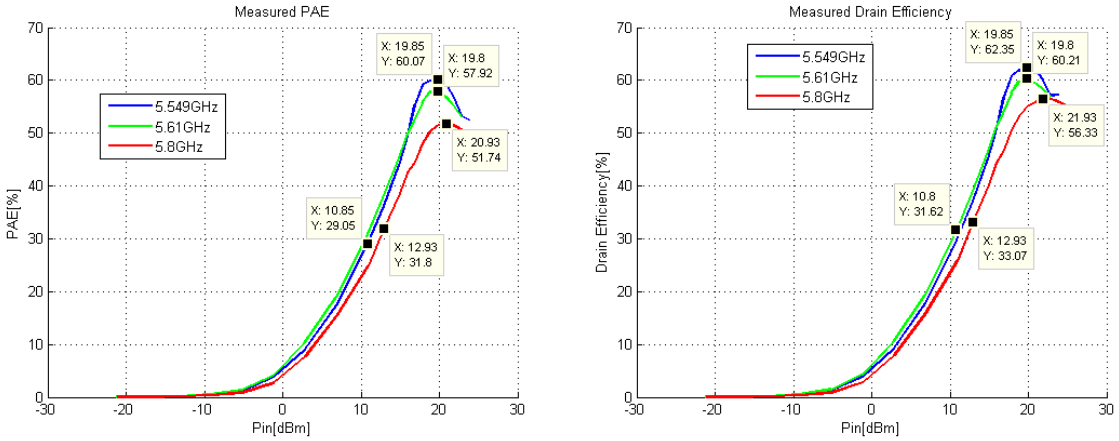

c) d)

Figure 71 - a) Transduction Gain, b) AM-AM, c) PAE and d) drain efficiency measurements

The microstrip PA can provide an output power of 27.8dBm (0.6W) at 1dB compression point for 5.549GHz and 5.61GHz and 34.1dBm (2.55W) at 5dB compression point, i.e., saturated. However, these values are lower than the output power achieved in simulation for 5.8GHz.

The small-signal gain measured is also 1.6dB lower than the gain predicted by the simulations (18.6dB). For this biasing point (class B), the simulations revealed a gain expansion of 1.3dB which do not occur in practice. In fact, at 0dBm of input power, the gain starts to compress and it seems much like the characteristic gain curve of a class AB. The gain compression justifies the lower drain efficiency (and gain) measured at 1dB compression point, 31.6% and 33.1% for 5.549GHz and 5.8GHz respectively, while in simulations it achieved 72%. At saturation, the drain efficiency improved, achieving 62.45%, 60.2% and 56.3% for 5.549GHz, 5.61GHz and 5.8GHz respectively.

The differences observed can be explained based on a few reasons. First, the technical limitations from the production process inserts important inaccuracies. As for this operation frequency, the lines width and length are already too reduced, each wrong cut by excess or defect may change the impedances.

On the other hand, the size of the bondwires is not controlled neither equally replicated because they are handmade. Thus, the bondwires have not the same size and also neither the size simulated in ADS (0.4mm).

Finally, it was confirmed by the results that the transistor model provided by Modelithics cannot reproduce the correct behavior of the transistor in real operation conditions. The datasheet of the transistor shows that load-pull curves simulated and measured are not coincident for some biasing points and frequencies, and the gain expansion showed in simulations did not happen in the measurements.

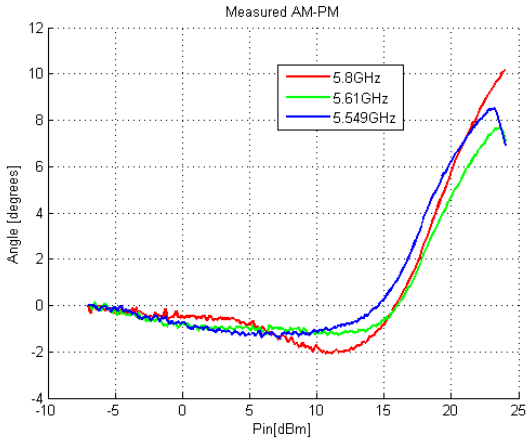

Figure 72 - AM-PM curve of the microstrip PA

The AM-PM curve measured for each frequency (figure 72) reveals a PA highly linear when it is evaluated the phase deflection provoked by the PA in amplified signals. It remains practically constant until the 1dB compression point (10-15dBm).

4.2.2. 2-tone measurements and modulated signals

The 2-tone measurements performed with the microstrip PA used the setup represented by the illustrative block diagram of the figure 73.

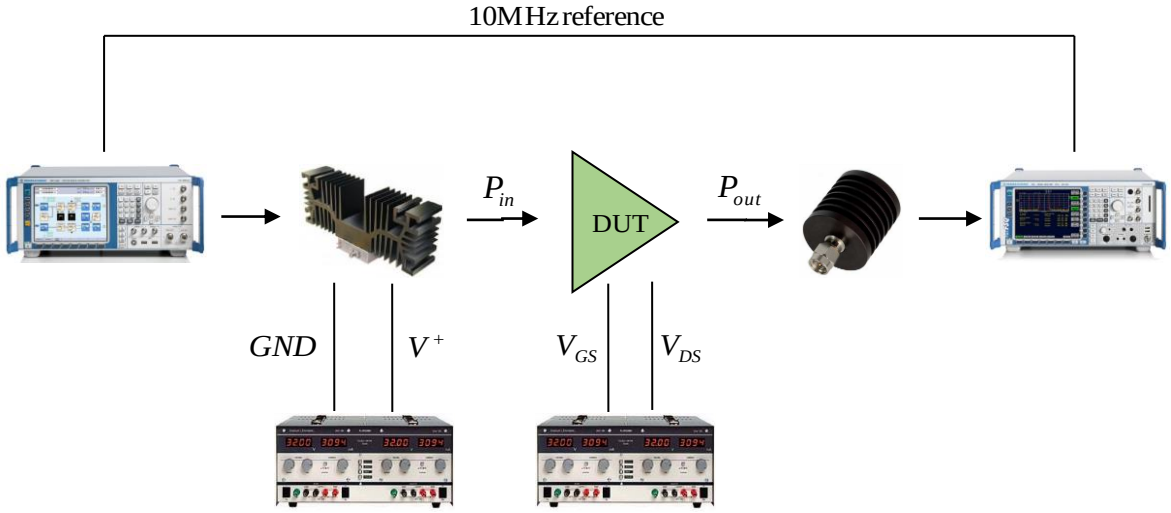

Figure 73 - Illustrative setup for 2-tone measurements

In order to assess the microstrip PA linearity, it was necessary to use a vector signal generator (VSG) and a vector spectrum analyzer (VSA), from Rohde & Schwarz, synchronized by a 10MHz reference, to perform the 2-tone tests varying the frequency spacing (100KHz,

1MHz, 5MHz and 10MHz) related to a carrier in 5.549GHz. The figure 74 shows a photo of the real setup used.

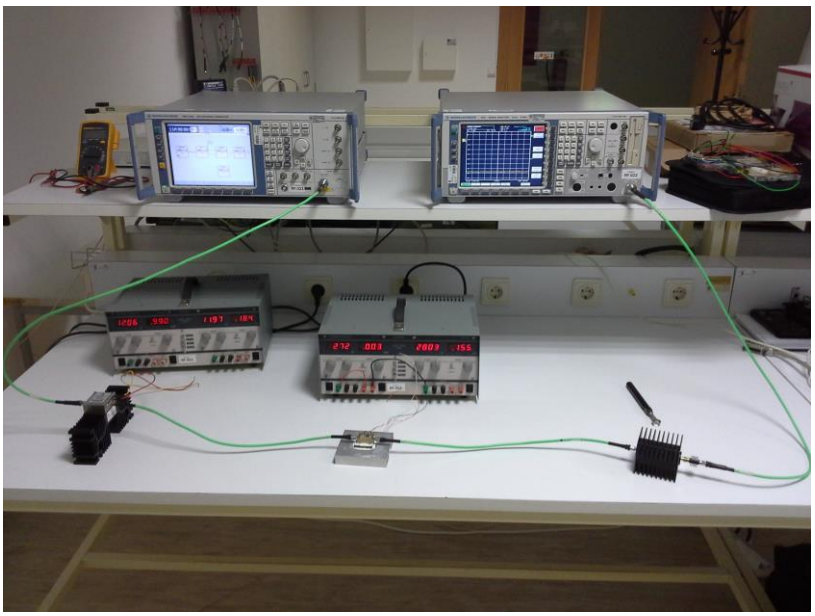

Figure 74 - Real setup for 2-tone measurements

These tests will allow to quantify the effect of the third order distortion component on the amplified signal and then, infer about the PA linearity through the IMR calculation.

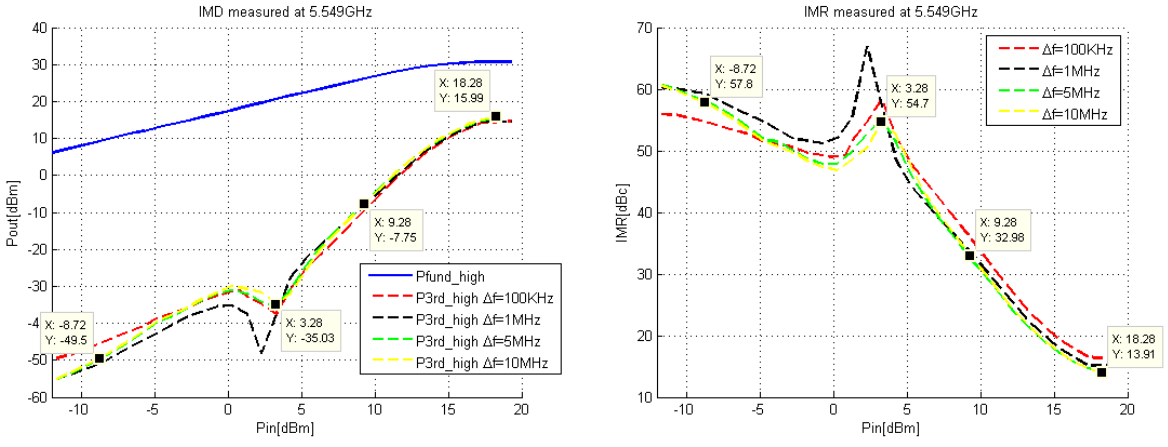

a) b)

Figure 75 - Measured a) IMD and b) IMR

From the figure 75 a), it can be highlighted the presence of a sweet spot, i.e. an IMD minimum, when the output power starts to compress. The IMD points are appealing to the RF engineers because the IMR of the PA improves (figure 75 b)) for the points near to the 1dB compression point. These valleys are consequence of the Gm_3 phase variations [82]. However, theory says that the class B has two sweet spots which it cannot be inspected through the data

presented in figure 75 a). Toward that point, one method that could be adopted to verify if there is a second sweet spot as expected to the class B biasing, consists on reduce the biasing current of the transistor, i.e., sweep the Vgs voltage to values lower than the first selected with the thinnest resolution possible on the power supply, and for each Vgs set, do another sweep for the input power and register again the output power and the IMD. Unfortunately, this process cannot be accomplished due to time constraints.

On the other hand, it may happen, the PA is truly biased in a class AB close to class B biasing, and the two sweet spots, verified in a typical class B, joined in the same point. So, the second sweet spot does not exist effectively and the PA was designed, after all, in a class AB biasing point. The last statement corroborates again the poor level of the transistor model.

The sweet spot more pronounced for a frequency spacing of the 1MHz can be an effect of the harmonic control performed in the PA design.

This work can proceed to the analysis of the PA behavior in terms of power transfer and data transmissions for WPT applications. For the first purpose, it can be analyzed the efficiency of the PA performing the DC to RF conversion in saturation points when excited with narrowband signals spaced among them (equidistant or not) of a few hundred kHz, as happens with the multisine signals. For the data transmissions, it can be measured for the highlighted input powers in the figure 75 a), the EVM provoked by the PA distortion in modulated signals (holding considerable bandwidths as 5MHz) which could be used in data transmission, such as PSKs and QAMs, and the generated power leakage in the adjacent frequency channels. Using again the setup illustrated in figure 73, the VSA can provide the necessary measurements.

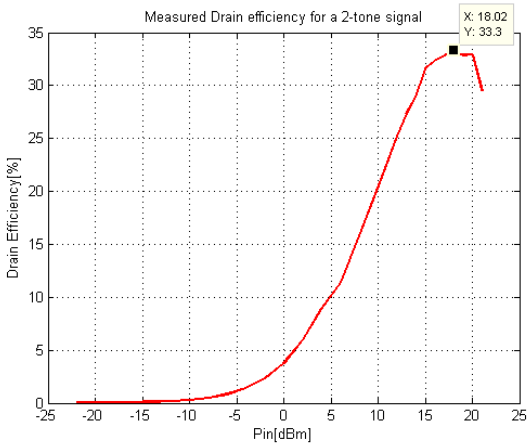

Figure 76 - Measured drain efficiency for a 2-tone signal with frequency spacing of 100kHz

Generating a 2-tone signal with frequency spacing of 100kHz in VSG, the PA achieves in saturation a drain efficiency of 33.3% (figure 76) which is approximately half of the drain efficiency showed when the PA was excited with a single tone signal (figure 71). It was predictable because the power is distributed equally between the two fundamental tones. In

power transfer applications for WPT, normally more than two tones are used (multisine signals) to achieve high PAPRs and then more power detected on receiver. So, this drain efficiency tends to be even lower when excited with these signals which it is not a favorable situation for system power requirements.

Table VIII - Modulated signals measurements

Modulated Signal	P_{in} (dBm)	EVM (%)	Mag. Error (%)	Phase Error (deg.)	$ACPR_{LO}$ (dB)	$ACPR_{UP}$ (dB)
QPSK	-8.7	2.88	2.05	1.15	42.21	42.07
	3.3	1.17	0.83	0.47	50.18	49.28
	9.3	1.38	0.83	0.63	41.32	40.72
	18.3	7.59	6.40	2.34	22.22	21.77
8-PSK	-8.7	2.81	1.97	1.15	43.56	42.97
	3.3	1.16	0.79	0.49	50.75	48.66
	9.3	1.45	0.87	0.66	40.90	39.80
	18.3	8.28	6.3	3.12	21.94	21.27
16-QAM	-8.7	2.86	1.5	1.6	42.22	42.08
	3.3	1.19	0.61	0.67	50.32	48.96
	9.3	2.56	0.99	1.55	37.22	36.39
	18.3	15.25	9.71	5.96	20.79	20.59
32-QAM	-8.7	2.78	1.5	1.69	43.02	42.95
	3.3	1.15	0.61	0.69	50.12	49.22
	9.3	2.18	0.89	1.42	37.48	37.08
	18.3	17.71	9.27	7.31	20.59	20.21

According to the table VIII, the collected data confirms the existence of a sweet spot detected in the two-tone measurements. As it can be seen, when the input power finds the sweet spot valley (input power of 3.3dBm), the distortion introduced by the power amplifier is lower and then, the magnitude and the phase error experienced by the modulated signals decrease as well. This effect is also sensed in the adjacent frequency channels which means that the power leakage to that channels falls too (see both ACPR columns). When the input power approaches the saturation levels, all modulated signals suffer the maximum distortion introduced by the PA and then, the error metrics soar significantly. Besides that, the modulation complexity influences highly the frequency of the errors occurrence. Thus, the used QAM modulations reveal errors higher than the PSK modulations.

Other phenomenon detected during the measurements, and presented in table VIII, is the asymmetries between the lower ACPR and the higher ACPR. This phenomenon could also be detected comparing the IMD high and the IMD low, which was not measured, and it is a result of the memory effects that the PA usually suffers. They are part of the PA dynamic behavior because they provoke changes in AM-AM and AM-PM responses of the PA [83]. So, the

memory effects cannot be neglected in data transmissions and must be characterized too, because they have a degradation impact on the PA linearity.

5. Conclusions and Future Work

5.1. Conclusions

The great motivation for this master thesis comes from the crescent maturation and exploitation of the GaN technology which have been sensed during the last decade to high power, efficiency and frequency applications such as satellite communications and WPT. GaN technology has a prominent position in this campaign because its characteristics predicts a better performance in applications of this nature when compared to other SSPAs technologies as GaAs.

After getting the knowledge about the state of the art of the GaN technology in satellite communications, it was proposed a implementation of two PAs for the 5.8GHz frequency, which can be used either for uplink transmissions in C-band, or used in WPT systems for power transmission or data links. Towards that point, the basic concepts inherent to the RF PAs were studied and also the figures of merit to evaluate the PA performance.

Two class B PAs were designed, one in microstrip lines and the other in CPW, in order to compare the performance of each planar transmission line under the same operation conditions, i.e., achieve at least 3W of output power and get the maximum drain efficiency from the active device at the 1dB compression point.

The microstrip line PA achieved in simulation 71.8% of drain efficiency and 35.1dBm of output power at 1dB compression point.

For the CPW implementation, it was necessary to design the t junctions, since the ADS CPW library does not have these discontinuities. The 1-tone HB simulation revealed a drain efficiency of 70.5% and 36.1dBm of output power at 1 dB compression point.

After the simulation stage, some work was performed in Autocad software in order to optimize the layouts before its implementation.

In an early stage of the tests, an S-parameters analysis were performed to both PAs, revealing a wideband PA for the microstrip implementation with the better gain and matching at 5.549GHz. On the other hand, as expected, the CPW implementation did not show relevant results and so, it was decided to not perform further tests. Thus, the CW, 2-tone and modulated signals tests were accomplished only for microstrip lines implementation.

At the 5.549GHz, it was achieved 31.6% of drain efficiency and 27.8dBm of output power at 1dB compression point and 62.4% of drain efficiency and 34.1dBm of output power at

saturation. The gain curve of this PA led to conclude that the PA designed with the chosen biasing point is a class AB and not a class B as indicated by the ADS simulations.

The 2-tone tests allowed to evaluate the distortion generated by the PA, where it was detected the presence of a sweet-spot which corroborated again that the designed PA is a class AB (close to class B). The drain efficiency measured with the 2-tone signal, approximately 33%, revealed the trend to high PAPR WPT signals.

Finally, the modulated signals (PSKs and QAMs) verified the good linearity of the PA, through the EVM and ACPR metrics, to data transmissions.

5.2. Future Work

As verified during the measurements, the transistor model provided by the Modelithics is not very accurate, specially the nonlinear characterization. So, one interesting future work would be to improve the ADS model of the transistor.

Later on, and following the last point, it could be implemented a PA according to the Doherty or the Envelope Tracking approaches to achieve a better performance in presence of high PAPR signals as the multisines used in WPT applications. Even more, a complete WPT transmitter could be implemented, including the latter PAs approaches.

Bibliography

[1] B. R. Elbert, *Introduction to Satellite Communications*. Artech House, 2008.

[2] D. J. Whalen, "Communication Satellites: Making the Global Village Possible", 2010. [Online]. Available: http://history.nasa.gov/printFriendly/satcomhistory.html.

[3] IEEE Global History Network, "John R. Pierce." [Online]. Available: http://www.ieeeghn.org/wiki/index.php/Oral-History:John_Pierce.

[4] IEEE Global History Network, "Harold A. Rosen." [Online]. Available: http://www.ieeeghn.org/wiki/index.php/Oral-History:Harold_Rosen.

[5] L. J. Ippolito, *Satellite Communications System Engineering*. Wiley, 2008.

[6] IEEE Global History Network, "Sputnik I." [Online]. Available: http://www.ieeeghn.org/wiki/index.php/Sputnik.

[7] IEEE Global History Network, "Nasa Launches TELSTAR." [Online]. Available: http://www.ieeeghn.org/wiki/index.php/NASA_Launches_Telstar.

[8] INTELSAT, "A Practical Introductory Guide on Using Satellite Technology for Communications", 2010. [Online]. Available: http://www.intelsat.com/wp-content/uploads/2013/01/5941-SatellitePrimer-2010.pdf.

[9] R. Emrick, P. Cruz, and N. B. Carvalho, "The Sky's the limit: Key Technology and Market Trends in Satellite Communications", *IEEE Microwave Magazine*, vol.15, no.6, pp. 65-78, 2014.

[10] Satnews, "TacSat-4 Makes Its Move", 2011. [Online]. Available: http://www.milsatmagazine.com/story.php?number=1137709048.

[11] G. Cavallaro, D. Pham-Minh, and M. Bousquet, "HEO Constellation Design for Tactical Communications", in *IEEE First AESS European Conference on Satellite Communications*, 2012.

[12] Y. J. Kenneth, *Satellite Communications Network Design and Analysis*. Artech House, 2011.

[13] B. R. Elbert, *Satellite Communications Application Handbook*. Artech House, 2004.

[14] A. D. Panagopoulos, P.-D. M. Arapoglou, and P. G. Cottis, "Satellite Communications at Ku, Ka and V bands: Propagation Impairments and Mitigation Techniques", *IEEE Commun. Surv. Tutorials*, vol. 6, no. 3, pp. 2–14, 2004.

[15] S. D. Turner and T. Dekker, "SSPA Technology Achieves 10 kW CW at S-Band", *IEEE Microw. J.*, vol. 55, no. 10, pp. 152–156, 2012.

[16] T. Ishida, “GaN HEMT Technologies for Space and Radio Applications”, *IEEE Microw. J.*, vol. 54, no. 8, pp. 56–61, 2011.

[17] C. F. Campbell, A. Balistreri, M.-Y. Kao, D. C. Dumka, and J. Hitt, “GaN Takes the Lead”, *IEEE Microwave Magazine*, vol.13, no.6, pp. 44–53, 2012.

[18] TriQuint Semiconductor, “New GaN FETs, Amplifiers and Switches Offer System Engineers a Way to Reduce RF Board Space and System Prime Power”, 2012. [Online]. Available: http://www.triquint.com/products/d/new-gan-fets-amplifiers-and-switches-improve-system-design.

[19] C. Langton, “Intuitive Guide to Principles in Communications”, 2013. [Online]. Available: http://complextoreal.com/wp-content/uploads/2013/01/twta.pdf.

[20] Satcom Resources, “MCL MT7100 TWTA Travelling Wave Tube High Power Amplifier.” [Online]. Available: http://www.satcomresources.com/MCL-MT7100-TWTA-Traveling-Wave-Tube-High-Power-Amplifier.

[21] Teledyne Microwave Solutions, “HPAs/TWT Amplifiers.” [Online]. Available: http://www.teledynemicrowave.com/index.php/teledyneproducts/teledyne-microwave-solutions-twts/twt-amplifiers.

[22] WTEC, “Transponders, HPAs and SSPAs.” [Online]. Available: http://www.wtec.org/loyola/satcom/c2_s2.htm.

[23] H. T. Than, G. W. Sun, G. S. Cuellar, and J. Zeng, “Design and Performance of a 600W C-Band Amplifier Using Spatially Combined GaAs FETs for Satellite Communications”, *IEEE J. Solid-State Circuits*, vol.47, no.10, pp. 2309–2315, 2012.

[24] De-Zhong Li, C. Wang, W.-C. Huang, and R. Krishna, “A high-power Ka-band power amplifier design based on GaAs P-HEMT technology for VSAT ODU applications”, in *IEEE International Symposium on Microwave, Antenna, Propagation and EMC Technologies for Wireless Communications*, 2009.

[25] F. Corporation, “State of the Satellite Industry Report,” 2012. [Online]. Available: http://www.futron.com/upload/wysiwyg/Resources/Reports/SSIR_2012.pdf.

[26] R. J. Trew, G. L. Bilbro, W. Kuang, and Y. Liu, “Microwave AlGaN/GaN HFETs”, *IEEE Microwave Magazine*, vol.6, no.1, pp. 56–66, 2005.

[27] M. Kameche and N. V. Drozdovski, “GaAs-, InP- and GaN HEMT-based Microwave Control Devices: What is Best and Why”, *IEEE Microw. J.*, vol. 48, no. 5, 2005.

[28] Advantech Wireless, “A New Generation of Gallium Nitride (GaN) based Solid State Power Amplifiers for Satellite Communication”, 2012. [Online]. Available: http://www.advantechwireless.com/wp-content/uploads/WP-A-new-generation-of-Gallium-Nitride.pdf.

[29] European Commission, “Eye on Space”, 2012. [Online]. Available: http://ec.europa.eu/rea/pdf/eyeonspace_4thcallspacebrochurenew.pdf.

[30] K. Takagi, K. Matsushita, Y. Kashiwabara, and K. Masuda, “Developing GaN HEMTs for Ka-Band with 20W”, in *IEEE Compound Semiconductor Integrated Circuit Symposium*, 2010.

[31] K. Takagi, N. Shinichiro, K. Masuda, and K. Matsushita, “GaN HEMTs with pre-match for Ka-Band with 18W”, in *IEEE International Microwave Symposium*, 2011.

[32] Toshiba Corporation, “Ka-Band High Power GaN MMIC”, 2012. [Online]. Available: http://www.toshiba.com/taec/news/press_releases/2012/mwrf_12_638.jsp.

[33] C. F. Campbell, M.-Y. Kao, and S. Nayak, “High efficiency Ka-band power amplifier MMICs fabricated with a 0.15μm GaN on SiC HEMT process”, in *IEEE International Microwave Symposium*, 2012.

[34] J. X. Qiu, A. M. Darwish, E. A. Viveiros, and H. A. Hung, “Linearity characteristics study of millimeter-wave GaN power amplifier”, in *IEEE International Microwave Symposium*, 2011.

[35] A. M. Darwish, J. X. Qiu, E. A. Viveiros, and H. A. Hung, “Improved linearity of power amplifier GaN MMIC for Ka-band Satcom”, in *IEEE International Microwave Symposium*, 2012.

[36] H. Shigematsu, Y. Inoue, A. Akasegawa, and M. Yamada, “C-band 340W and X-band 100W GaN power amplifiers with over 50% PAE”, in *IEEE International Microwave Symposium*, 2009.

[37] K. Yamauchi, H. Noto, H. Nonomura, and S. Kunugi, “A 45% power added efficiency, Ku-band 60W GaN power amplifier”, in *IEEE International Microwave Symposium*, 2011.

[38] J. Harvey, E. R. Brown, D. B. Rutledge, and R. A. York, “Spatial power combining for high-power transmitters”, *IEEE Microwave Magazine*, vol.1, no.4, pp. 48–59, 2000.

[39] CAP Wireless, “Spatial Combining Technology: Revolutionizing the Microwave Power Amplifier”, *IEEE Microwave Journal*, 2008.

[40] J. Schellenberg, E. Watkins, M. Micovic, and B. Kim, “W-band, 5W solid-state power amplifier/combiner”, in *IEEE International Microwave Symposium*, 2010.

[41] H. Noji, Y. Shibuya, K. Isono, and M. Hori, “A 1kW-class S-band compact waveguide combiner unit with GaN HPAs for WPT and space communication”, in *European Microwave Conference*, 2011.

[42] World Broadcasting Unions, “C-band frequencies Are Under Threat - Join Our Efforts to Safeguard C-band Spectrum!”, 2013. [Online]. Available: http://www.worldbroadcastingunions.org/wbuarea/library/docs/isog/CASBAA C-band Appeal to Broadcasters.pdf.

[43] S. Kawasaki, “Compact, Planar and High-Power Spatial Power Combiner by Active Integrated Antenna Technique at 5.8 GHz”, in *Korea-Japan Microwave Conference*, 2007.

[44] S. Kawasaki, U. Gokasho, S. Kawai, T. Yamamoto, and K. Takei, “A 5.8GHz-Band Active Integrated Phased Array Antenna with Wireless Communication and Power Transmission Functions for Space and Satellite Use”, in *China-Japan Joint Microwave Conference*, 2008.

[45] K. Honjo, R. Ishikawa, and Y. Takayama, “Ultra high efficiency microwave power amplifier for wireless power transmission”, in *European Microwave Conference*, 2012.

[46] C. Bergsrud, S. Noghanian, J. Straub, and D. Whalen, “Orbit-to-ground Wireless Power Transfer test mission”, in *Aeorspace Conference*, 2013.

[47] J. L. B. Walker, *Handbook of RF and Microwave Power Amplifiers*. Cambridge University Press, 2012.

[48] J. C. Pedro and N. B. Carvalho, *Intermodulation Distortion in Microwave and Wireless Circuits*. Artech House, 2004.

[49] M. Golio and J. Golio, *RF and Microwave Circuits, Measurement and Modelling*. CRC Press, 2008.

[50] H. L. Krauss, C. W. Bostian, and F. H. Raab, *Solid State Radio Engineering*. Wiley, 1980.

[51] Luís C. Cótimos, “Amplificador em Classe F para Sistemas de Transmissão Polar,” Aveiro, 2010.

[52] D. M. Pozar, *Microwave Engineering*. Wiley, 2012.

[53] P. Colantonio, F. Giannini, and E. Limiti, *High Efficiency RF and Microwave Solid State Power Amplifiers*. Wiley, 2009.

[54] P. J. Baxandall, “Transistor sine-wave LC oscillators. Some general considerations and new developments”, in *Electronic and Communication Engineering Proceedings of the IEEE*, 1959.

[55] F. H. Raab, P. Asbeck, S. Cripps, and P. B. Kenington, “Power amplifiers and transmitters for RF and microwave”, *IEEE Microw. Theory Tech.*, vol. 50, no. 3, pp. 814–826, 2002.

[56] A. Grebennikov and N. O. Sokal, *Switchmode RF Power Amplifiers*. Elsevier, 2007.

[57] N. O. Sokal and A. D. Sokal, “Class E-A new class of high-efficiency tuned single-ended switching power amplifiers”, *IEEE J. Solid-State Circuits*, vol. 10, no. 3, pp. 168–176, 1975.

[58] R. Pengelly, D. Holmes, M. Acar, R. Wesson, and M. P. van der Heijden, “Modern High Efficiency Amplifier Design: Envelope Tracking, Doherty and Outphasing Techniques”, *IEEE Microwave Journal*, 2014.

[59] Xilinx, “Digital Predistortion.” [Online]. Available: http://www.xilinx.com/products/intellectual-property/EF-DI-DPD.htm.

[60] A. Collado and A. Georgiadis, “Improving wireless power transmission efficiency using chaotic waveforms”, in *IEEE International Microwave Symposium Symposium Digest*, 2012.

[61] A. S. Boaventura and N. B. Carvalho, “Maximizing DC power in energy harvesting circuits using multisine excitation”, in *IEEE International Microwave Symposium Digest*, 2011.

[62] A. J. S. Boaventura, A. Collado, A. Georgiadis, and N. Borges Carvalho, “Spatial Power Combining of Multi-Sine Signals for Wireless Power Transmission Applications”, in *IEEE Microwave Theory and Techniques*, 2014.

[63] W. H. Doherty, “A New High Efficiency Power Amplifier for Modulated Waves”, *IEEE Radio Eng.*, vol. 24, no. 9, pp. 1163–1182, 1936.

[64] L. Frenzel, “Envelope Tracking Technology Boots RF PA Linearity and Efficiency”, 2013. [Online]. Available: http://electronicdesign.com/power/envelope-tracking-technology-boosts-rf-pa-linearity-and-efficiency.

[65] G. Wimpenny, “Understand and characterize envelope-tracking power amplifiers”, 2012. [Online]. Available: http://edn.com/design/analog/4372705/Understand-and-characterize-envelope-tracking-power-amplifiers-item-2.

[66] P. Lavrador, T. R. Cunha, P. Cabral, and J. C. Pedro, “The Linearity-Efficiency Compromise”, *IEEE Microwave Magazine*, vol.11, no.5, pp. 44–58, 2010.

[67] H. Seidel, “A Feedforward Experiment Applied to an L-4 Carrier System Amplifier”, *IEEE Transactions on Communication Technology*, 1971.

[68] M. K. Kazimierczuck, *RF Power Amplifier*. Wiley, 2008.

[69] A. A. M. Saleh and J. Salz, “Adaptive linearization of power amplifiers in digital radio systems”, *Bell Syst. Tech. J.*, vol. 62, no. 4, pp. 1019–1033, 1983.

[70] Empfasis, “Antenna Combining,” 2010. [Online]. Available: http://www.empf.org/empfasis/2010/June10/antenna.html.

[71] TriQuint Semiconductor, “TGF2023-2-01.” [Online]. Available: http://www.rfmw.com/ProductDetail/TGF2023201-TriQuint/460920/.

[72] Rogers Corporation, “Duroid 6010.” [Online]. Available: http://www.rogerscorp.com/documents/612/acm/RT-duroid-6006-6010-laminate-data-sheet.aspx.

[73] P. M. Cabral, “Nonlinear Modelling of Power Transistors for RF and Microwaves”, 2006.

[74] L. G. Maloratsky, *Passive RF & Microwave Integrated Circuits*. Elsevier, 2004.

[75] CSR, “An Introduction to Antennas and Propagation”, 2011. [Online]. Available: http://www.csr.com/introduction-antennas-and-propagation-part-3.

[76] I. Wolff, *Coplanar Microwave Integrated Circuits*. Wiley, 2006.

[77] C. P. Wen, “Coplanar waveguides: A surface strip transmission line suitable for nonreciprocal gyromagnetic devices applications”, *IEEE Microw. Theory Tech.*, vol. 17, no. 12, pp. 1087–1090, 1969.

[78] M. Houdart, “Coplanar lines: Application to broadband microwave integrated circuits”, in *European Microwave Conference*, 1976, pp. 49–53.

[79] R. M. Simons, *Coplanar Waveguide Circuits, Components and Systems*. Wiley, 2001.

[80] J. Coonrod and B. Rautio, “Comparing Microstrip and CPW Performance”, *IEEE Microwave Journal*, vol. 55, no. 74–82, 2012.

[81] E. Ersoy, C. Meliani, S. Chevtchenko, and P. Kurpas, “A High-Gain X-Band GaN-MMIC Power Amplifier”, in *German Microwave Conference*, 2012, pp. 1–4.

[82] N. B. Carvalho and J. C. Pedro, “Large- and Small-Signal IMD Behavior of Microwave Power Amplifiers”, *IEEE Microw. Theory Tech.*, vol. 47, no. 12, pp. 2364–2374, 1999.

[83] J. Gering, “Large-Signal Measurements for Power Amplifier (PA) Characterization”, *IMS Workshop WHS*, 2008. [Online]. Available: http://www.rfmd.com/cs/documents/COMMJGeringIMS08.pdf.

Appendix A

Short Letter from IEEE MTT-S Society

Microwave Theory and Techniques Society (MTT-S) Education Committee

February 10, 2014

Dear Awardee,

On behalf of the MTT-S Education Committee I would like to congratulate you on being selected to receive an MTT-S Undergraduate/Pre-graduate Scholarship for Spring 2014.

The award consists of:

a. A certificate of recognition. There is a Student Awards Luncheon held on Thursday at every IMS conference to recognize student contributions to the MTT-S Society. You are cordially invited to attend with your mentor the IMS 2014 Student's Luncheon on Thursday, June 5, 2014 in Tampa Bay, FL, USA to receive your certificate. If you are unable to attend, the certificate will be mailed to you after the conference or alternative arrangements will be made to deliver it to you.

b. A scholarship of $1500 USD.

c. A travel reimbursement (up to $1000 USD) to attend IMS 2014 or an MTT-S sponsored conference. The travel supplement is available upon request to the Scholarship Chair to attend the conference. The request will need to be approved by your Mentor and submitted to the Scholarship Chair prior to attendance for approval. Note that this additional financial support does not include expenses related to registering for the conference.

d. One year IEEE and MTT-S student membership.

The instructions on the next steps will be sent to you soon.

Again, congratulations and thank you for participating in the IEEE MTT-S Undergraduate /Pre-graduate Scholarship program.

Sincerely,

Zlatica Marinković

Dr. Zlatica Marinković
MTT-S Education Committee,
Undergraduate Scholarships Chair